The Presidents' Day Cyclone of 18–19 February 1979: Synoptic Overview and Analysis of the Subtropical Jet Streak Influencing the Pre-Cyclogenetic Period

LOUIS W. UCCELLINI, PAUL J. KOCIN AND RALPH A. PETERSEN

Goddard Laboratory for Atmospheric Sciences, NASA/Goddard Space Flight Center, Greenbelt, MD 20771

CARLYLE H. WASH

Department of Meteorology, Naval Postgraduate School, Monterey, CA 93940

KEITH F. BRILL

General Software Corporation, Landover, MD 20785

(Manuscript received 9 September 1982, in final form 8 August 1983)

ABSTRACT

The Presidents' Day cyclone of 18–19 February 1979 was an intense and rapidly developing storm which produced heavy snowfall along the East Coast of the United States. An analysis of the cyclone is presented which isolates three jet streaks that appear to have played important roles in the development of two separate areas of heavy snow. One area of heavy snow developed prior to cyclogenesis and is linked, in part, to an increasingly unbalanced subtropical jet streak (STJ) and a noticeably ageostrophic low-level jet. The second area of heavy snow developed in conjunction with the explosive cyclogenesis off the East Coast as a polar jet streak and midtropospheric trough propagated toward the coastal region from the north-central United States.

This paper examines the STJ in detail. The maximum wind speeds associated with the STJ increased by 15 to 20 m s^{-1} between 1200 GMT 17 and 1200 GMT 18 February 1979 as the jet propagated from the south-central toward the eastern United States. During the 24 h period, the flow in the STJ became increasingly supergeostrophic and apparently unbalanced. Ageostrophic wind speeds increased to greater than 30 m s^{-1}, with a significant cross-contour component directed toward lower values of the Montgomery streamfunction, as the flow along the STJ became increasingly divergent with time. The increased wind speed, ageostrophic flow, and divergence along the axis of the STJ are linked to the increasing confluence in the entrance region of the jet streak and the decreasing wavelength of the trough–ridge system in which the jet streak was embedded. The upper level divergence and upward vertical motion near the axis of the STJ along with the moisture transport associated with the LLJ are found to be important factors in the development of the first area of heavy snow.

1. Introduction

On 18–19 February 1979, a very intense cyclone developed along the Middle Atlantic Coast which produced 45 to 60 cm of snow from Virginia to southern New Jersey, including the greatest 24 h snowfall accumulation in Washington, D.C., in over 50 years (Foster and Leffler, 1979). The storm, referred to as the Presidents' Day cyclone, is of particular interest because of its intensity, the apparent contribution of many physical processes to its rapid development on 19 February 1979, and the failure of the National Meteorological Center's (NMC) operational Limited Area Fine Mesh model (LFM-II) to forecast accurately the cyclogenesis and heavy snowfall.

In an analysis of the Presidents' Day storm, Bosart (1981) places particular emphasis on describing the coastal frontogenesis observed prior to cyclone development and the extent to which boundary-layer processes and diabatic processes contributed to the rapid cyclogenesis. Nevertheless, other studies have shown that jet streaks[1] often play an important role in the development of cyclones (e.g., Newton, 1956; Reiter, 1969; Hovanec and Horn, 1975). The intent of this paper is to determine the role of upper- and lower-tropospheric jets before and during the period of rapid cyclogenesis.

The specific purposes of this paper are: 1) to present a synoptic overview of the Presidents' Day cyclone that isolates two distinct periods of heavy snow, 2) to identify the subtropical, polar, and low-level jet streaks which appear to have influenced the development of the cyclone, and 3) to focus on the subtropical jet streak (STJ) and its role in the development of the first area of heavy snow in the southeastern United States during the pre-cyclogenetic period. In Section

[1] Palmén and Newton (1969, p. 199) define jet streaks as the regions of isotach maxima embedded within the jet stream.

© 1984 American Meteorological Society

2, synoptic analyses are presented to provide a general overview. Detailed diagnostic analyses highlighting the STJ are presented in Section 3. Emphasis will be placed on the significant departure of the flow in the STJ from geostrophic balance and on other indications of unbalanced flow along the axis of the jet. In Section 4, the mass adjustment and indirect transverse circulation associated with the STJ are discussed and related to the development of an area of heavy snow. In Section 5, the results of the study are summarized and questions regarding future research are discussed. Future papers will deal with a diagnosis of the other jet systems identified in the synoptic overview.

2. A Synoptic overview

Analyses derived from conventional surface and radiosonde data are presented in Figs. 1 through 6 for the period 1200 GMT 17 February 1979 through 1200 GMT 19 February 1979 to provide a synoptic overview of the Presidents' Day cyclone. Henceforth, the times (GMT) and dates of synoptic observations within this period will be referenced as 12Z/17, 00Z/18, 12Z/18, 00Z/19, and 12Z/19. Since isobaric analyses have been provided already by Bosart (1981), analyses on isentropic surfaces are presented to provide an alternative perspective from which to view the jet streak processes. The isentropic framework is better suited for the study of jets since jet streaks tend to follow an isentropic surface (Newton and Persson, 1962). The isentropic framework also provides a coherent, three-dimensional depiction of upper-, middle-, and lower-tropospheric flow regimes from the perspective of two-dimensional charts (e.g., Oliver and Oliver, 1951; Uccellini, 1976; Carlson, 1980). Furthermore, the isentropic coordinate system offers a means for more accurate trajectory computations (Danielsen, 1961; Petersen and Uccellini, 1979), which are an important aspect of this case study.

The isentropic analyses presented in this section and used for the detailed diagnostic study in Section 3 were generated by an objective analysis scheme developed by Petersen (1979). The analysis scheme is unique in that it interpolates pressure, wind, and moisture information from vertical cross sections onto isentropic surfaces using cubic polynomials. Therefore, detailed information included within the vertical structure of sets of individual soundings is incorporated objectively within the analysis to capture significant horizontal thermal gradients associated with jet systems. To improve the spatial and temporal continuity of the analyzed wind fields, a modification has been applied to the wind analysis procedure. Rather than using the geostrophic wind as a first guess, a broad area one-pass Cressman analysis of the ratio of the observed wind speed to the geostrophic wind speed at the stations is computed to yield a modified first guess wind field that contains supergeostrophic and subgeostrophic wind speeds in ridges and troughs, respectively. As a result, the ageostrophic wind components in the final wind analysis appear to be more realistic and coherent than when using a geostrophic first guess. The objective analyses agree with the subjective analyses presented by Uccellini *et al.* (1981) and are therefore used for the detailed diagnostic computations presented in Section 3.

Carefully checked radiosonde data were used over the United States, while eight oceanic supplemental soundings were constructed within 1000 km of the Southeast Coast to extend the analysis domain eastward and set boundary values for the analysis scheme (Fig. 2C1). The supplemental soundings were constructed from the NMC surface and upper-level analyses on the mandatory pressure levels.

Wind, moisture, and pressure analyses were derived on a 2° by 2° latitude–longitude grid for isentropic surfaces extending from 272 K to 340 K at 4 K increment. The 292, 312 and 332 K surfaces are shown here. The 292 K surface is representative of the lower troposphere over the southeastern United States, where a strong low-level jet developed by 12Z/18. The 312 K surface slopes from the middle to the upper troposphere and passes through a layer within which a polar jet propagated toward the East Coast and intensified by 00Z/19. The 332 K surface nearly parallels the tropopause level over the southeastern United States and provides a reference level for examining the subtropical jet analyzed over the southeastern United States during the entire observing period.

a. Surface and upper air analyses

At 12Z/17, a massive high pressure system centered over Lake Superior (Fig. 1A) was marked by record low surface temperatures from southern Canada to the eastern United States. Aloft, an intense polar jet over the northeastern United States was propagating towards the North Atlantic (Figs. 2B1 and 2C1). A subtropical jet streak (STJ) extended from Texas toward the Ohio Valley, east of a trough over the Rocky Mountains (Fig. 2A1). While the polar jet was most pronounced near 350 mb on the 312 K surface (Fig. 2B2), the STJ was maximized near 215 mb on the 332 K surface (Fig. 2A2), consistent with the expectation of a higher tropopause for subtropical jets (Krishnamurti, 1961).

At 00Z/18 (Fig. 1B), the large surface anticyclone remained over the Great Lakes. A high pressure ridge moved southward along the East Coast, reflecting the "damming" of cold air east of the Appalachian Mountains (Richwien, 1980). Snow and sleet had developed over the southern United States, with the first indication of an inverted trough extending northward from the Gulf of Mexico. Mixing ratio analyses on the two lower isentropic surfaces (Figs. 3B2 and 3C2) indicate an increasing amount of moisture in the Gulf Coast region coincident with the expanding precipitation shield. Maximum winds associated with the STJ in-

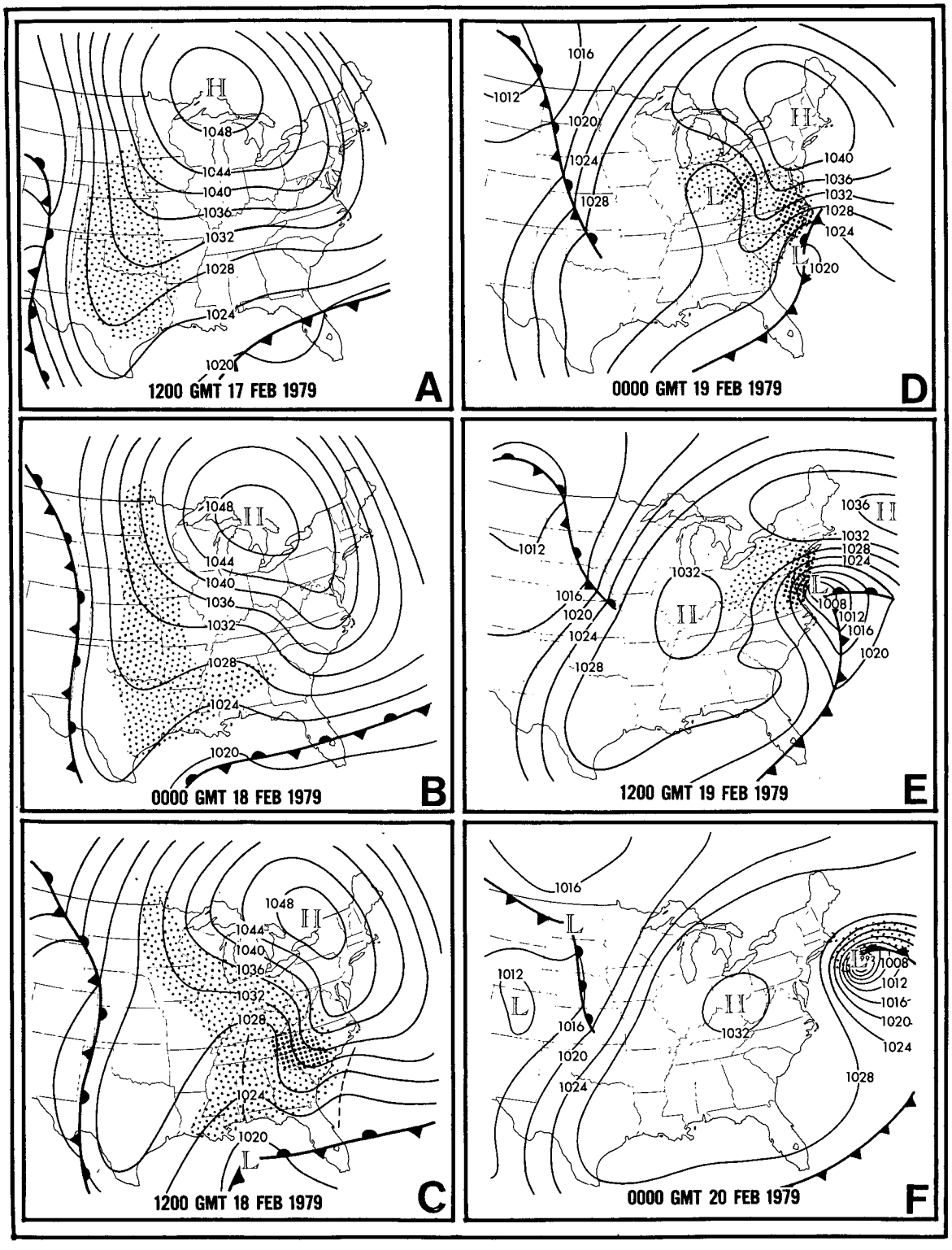

FIG. 1. Sea-level pressure (mb) and surface frontal analyses for (A) 1200 GMT 17 February; (B) 0000 GMT 18 February; (C) 1200 GMT 18 February; (D) 0000 GMT 19 February; (E) 1200 GMT 19 February; and (F) 0000 GMT 20 February 1979. Shading represents precipitation; dark shading indicates moderate to heavy precipitation. Dashed lines in (C) denote inverted and coastal troughs.

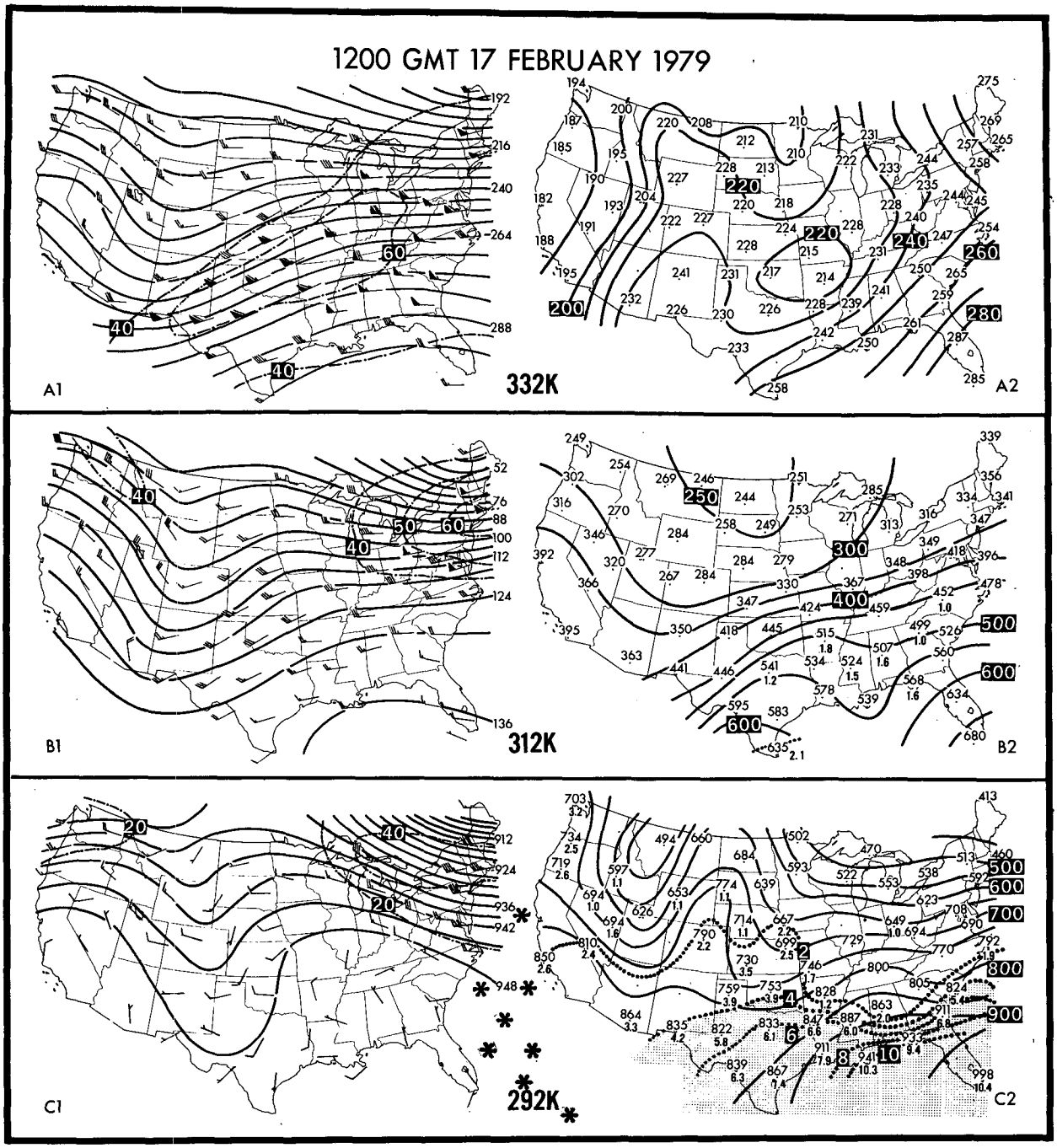

FIG. 2. Isentropic analyses for 1200 GMT 17 February 1979 for 332 K (A1), 312 K (B1), and 292 K (C1) surfaces. Montgomery streamfunction (ψ_m) analysis (solid, 240 = 3.240×10^5 m^2 s^{-2}; 936 = 2.936×10^5 m^2 s^{-2}) and isotachs (dot–dash, m s^{-1}). Wind barbs represent observed speeds (whole barbs denote 10 m s^{-1}; half barbs denote 5 m s^{-1}). Pressure (solid, mb) and mixing ratio (dotted, g kg^{-1}) for 332 K (A2), 312 K (B2), and 292 K (C2). Shading represents mixing ratios > 4 g kg^{-1}. Asterisks in C1 represent locations of supplemental sounding sites off the East Coast.

creased from less than 70 m s^{-1} at 12Z/17 (Fig. 2A1) to 75 m s^{-1} by 00Z/18 (Fig. 3A1) as the upper-level trough propagated east-northeastward through the central United States. At intermediate levels, the 312 K analyses show a polar jet streak (PJ) propagating southeastward across Montana between 250 and 300 mb (Figs. 3B1 and 3B2). This PJ was situated upwind of the trough and later became an important element of the cyclogenetic process.

By 12Z/18, moderate to heavy snow developed in

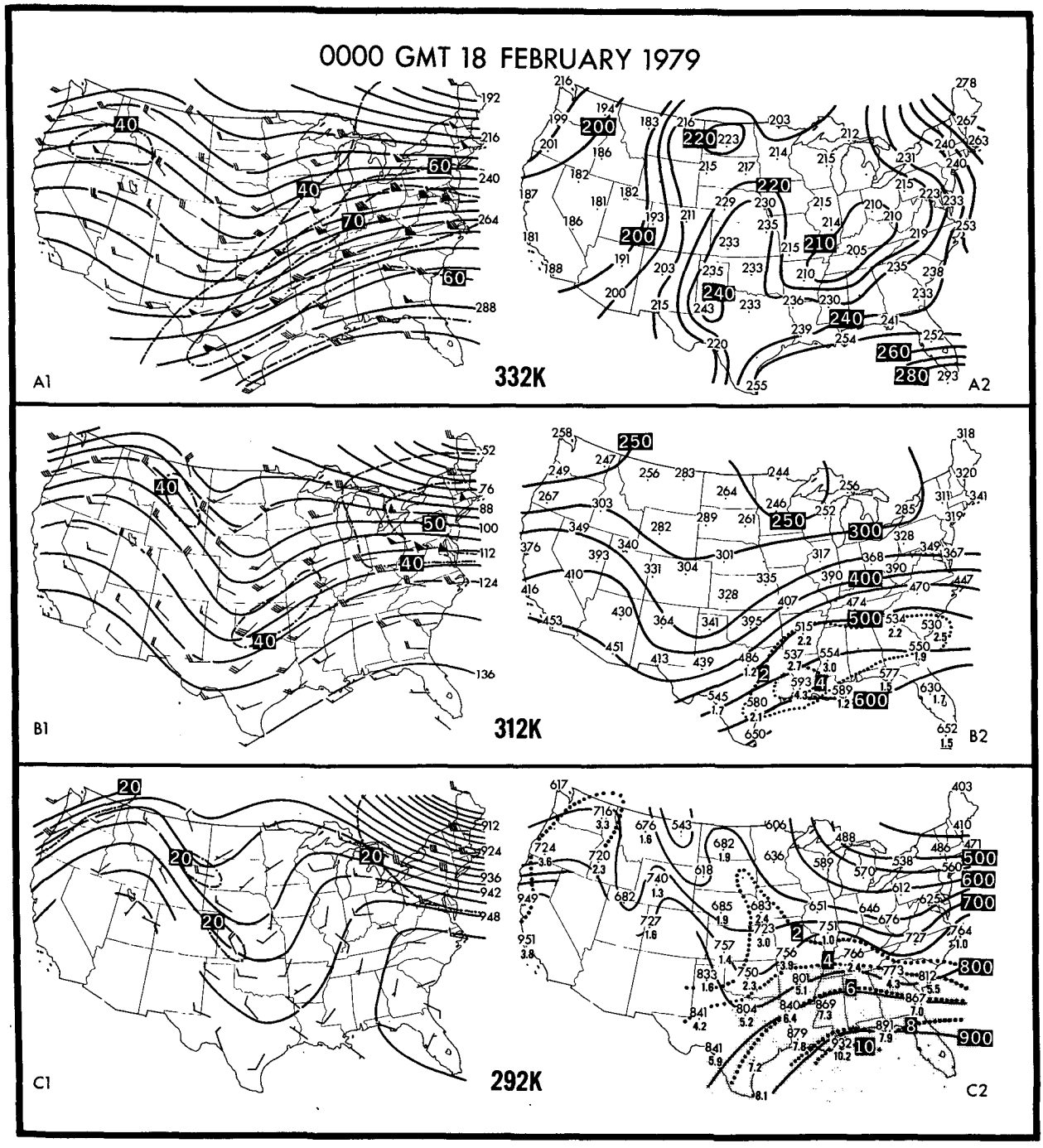

FIG. 3. As in Fig. 2 but for 0000 GMT 18 February 1979.

the southern Appalachians as the inverted surface trough extended northward from the Gulf of Mexico and became more pronounced, while a separate trough began to develop off the Southeast Coast (Fig. 1C). Some noteworthy changes were also observed in both the upper- and lower-tropospheric wind fields. First, the maximum winds along the axis of the STJ and near the ridge axis continued to increase and were now generally between 75 and 80 m s^{-1} (Fig. 4A1). As the wind speeds become large in the upper troposphere, the wind measurements become less accurate due to errors related to the large elevation angle (e.g., see Newton and Persson, 1962). Therefore, it is difficult to determine if the magnitude of the STJ actually approached 90 m s^{-1} as indicated by the wind report at Greensboro, North Carolina, at 12Z/18 (Fig. 4A1).

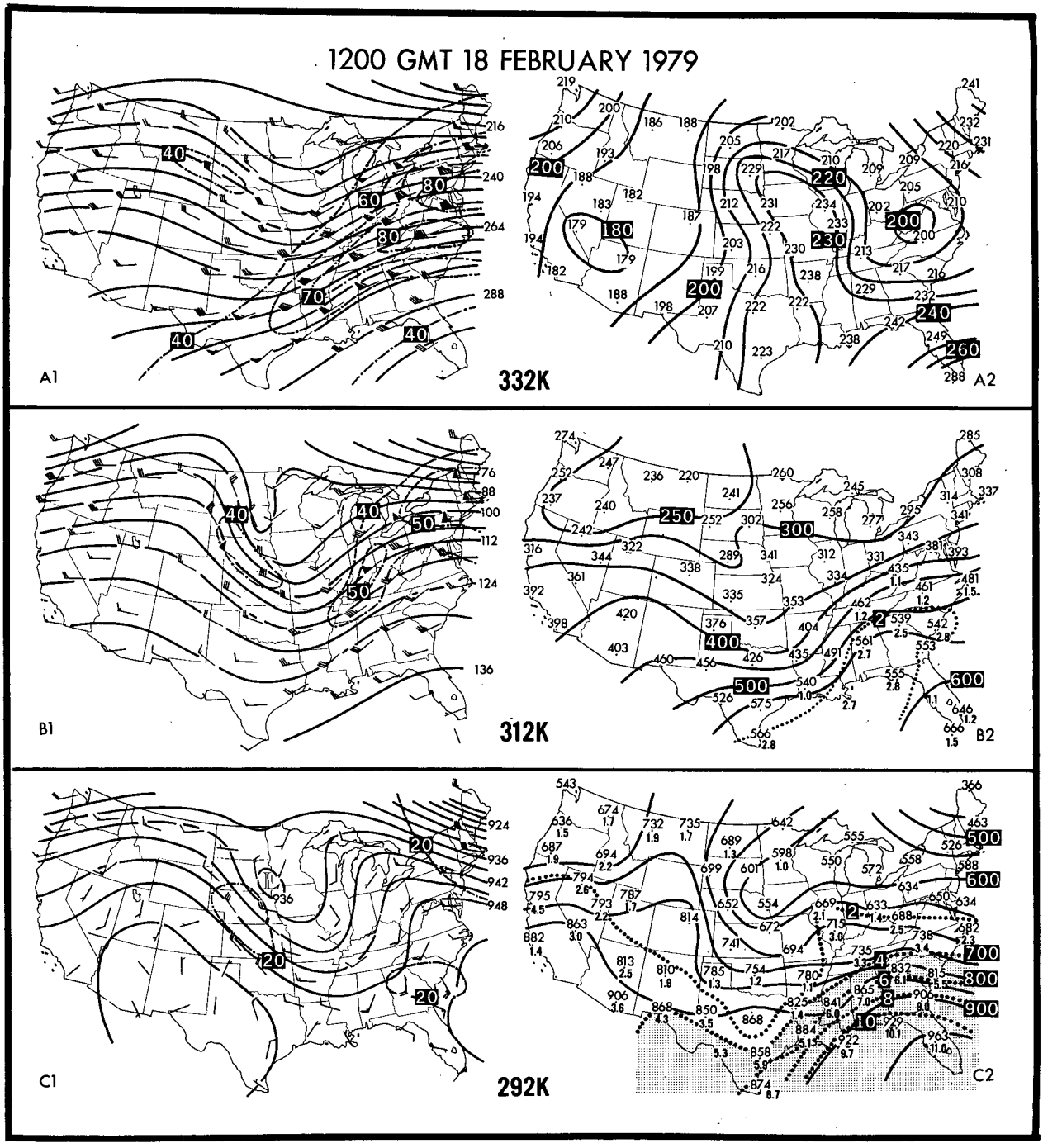

FIG. 4. As in Fig. 2 but for 1200 GMT 18 February 1979.

Nevertheless, wind speeds increased from 3 to >10 m s^{-1} at nearly all the stations along the axis of the STJ between 00Z/18 and 12Z/18. The increase of the maximum winds in the STJ between 12Z/17 and 12Z/18 occurred as the distance between the slowly moving ridge and the more rapidly propagating trough decreased, as indicated on the 332 K surface (Fig. 10B). Second, a noticeably ageostrophic low-level jet (LLJ) developed in South Carolina and Georgia, as south to southeasterly wind speeds increased to as high as 25 m s^{-1} on the 292 K surface with wind directions nearly normal to the Montgomery stream function (ψ_m) contours (Fig. 4C1). The LLJ was located south of the STJ and extended well beyond the planetary boundary layer to 750 mb (Fig. 4C2). The LLJ appears to have enhanced the moisture transport into the region of

moderate to heavy snowfall, and also provided a potential lifting mechanism due to cross-isobaric flow up the steeply sloped isentropic surfaces (Fig. 4C2). Third, the PJ continued to propagate toward the Midwest, approaching the axis of the amplifying short-wave trough at the 312 K level (Fig. 4B1).

By 00Z/19, the strong surface ridging along the Atlantic coastal plain (Fig. 1D) accompanied the entrenchment of record-breaking cold air east of the Appalachian Mountains (Foster and Leffler, 1979). Weak surface lows formed along the coastal front near Georgia and in the inverted trough in the Ohio Valley. Heavy snowfall was occurring northwest of the coastal low and northeast of the Midwest surface low. Aloft,

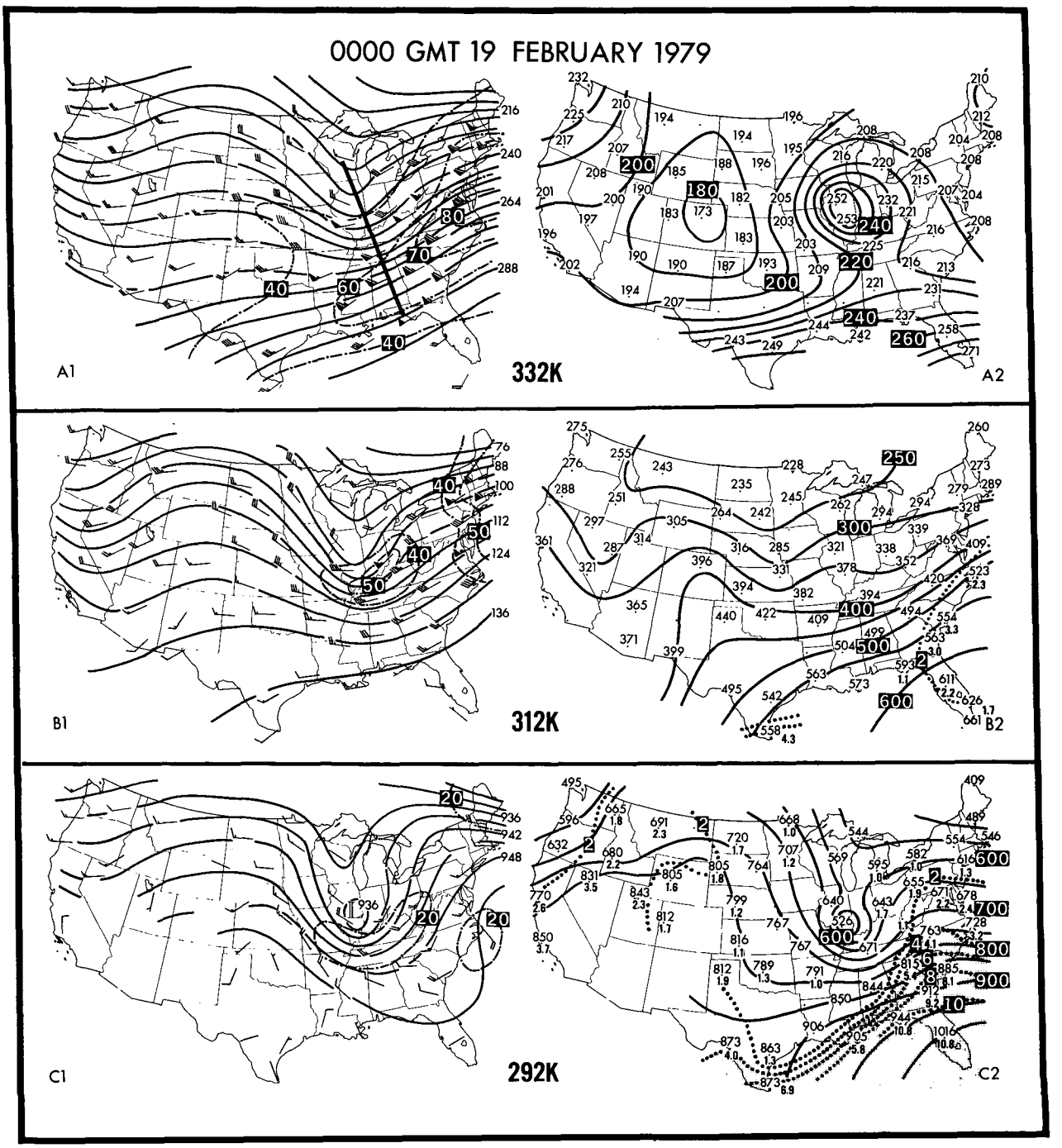

FIG. 5. As in Fig. 2 but for 0000 GMT 19 February 1979. Line in (5A1) indicates position of cross section shown in Fig. 6.

the STJ continued to propagate off the East Coast with a maximum wind speed remaining above 80 m s^{-1} (Fig. 5A1). The PJ was now intensifying, with wind speeds increasing to greater than 50 m s^{-1} at the 312 K level, as it propagated into the base of the trough (Fig. 5B1). The trough over the Midwest also amplified, with the magnitude of the ψ_m gradients and curvature near the base of the trough increasing at all levels (Figs. 5A1, 5B1 and 5C1). This PJ–trough system was beginning to provide the quasi-geostrophic forcing for East Coast cyclogenesis discussed by Bosart (1981). By 00Z/19, the LLJ remained noticeably ageostrophic at 292 K as it propagated northeastward along the coast (Fig. 5C1) and again appeared to be transporting moisture toward the region of heavy snowfall located along the East Coast (Fig. 1D).

To illustrate further the distinct characteristics of the PJ and STJ, a vertical cross section was constructed from Green Bay, Wisconsin, to Appalachicola, Florida, at 00Z/19 as indicated by the solid line in Fig. 5A1. The cross section includes total wind speeds (Fig. 6A), isentropes, geostrophic wind speeds, and potential vorticity (Fig. 6B). The potential vorticity was computed on a three-dimensional array of grid points using the expression, $-(\zeta_\theta + f)\partial\theta/\partial p$, and interpolated linearly to the plane of the cross section. The cross sections of the total and geostrophic wind speeds (Figs. 6A and 6B) clearly show the separation of the 55 m s^{-1} PJ maximized near the 312 K level just below 300 mb from the STJ maximized near the 332 K level just above 200 mb. A distinct maximum in the component of the geostrophic wind normal to the plane of the cross section (U_g) was diagnosed for each jet (Fig. 6B), with U_g maximized between 300 and 500 mb for the PJ and near 200 mb for the STJ. The midtropospheric frontal zone associated with the PJ was marked by a significant vertical shear in U_g between 700 and 500 mb just north of Nashville, Tennessee (BNA, Fig. 6B). In contrast, the vertical shear associated with the STJ was weaker and spread through a deeper layer in the middle and upper troposphere. These observations of the separate PJ and STJ are consistent with Newton and Persson's (1962) analysis of subtropical and polar jets. The potential vorticity is included as another indication of the intensification of the PJ–trough system (Fig. 6B). The extrusion of high values of potential vorticity (exceeding 10^{-5} K s^{-1} mb^{-1}) downward to the 700 mb level near Salem, Illinois (SLO), and BNA occurred within the midtropospheric frontal zone between 00Z/18 and 12Z/18 (not shown). The potential vorticity structure and magnitude in Fig. 6B resemble those of Reed and Danielsen (1959) and Shapiro (1976), suggesting that a "tropopause fold" (Reed and Danielsen, 1959; Staley, 1960) had occurred within the frontal zone by 00Z/19 as the PJ–trough system propagated toward the Ohio Valley. The stratospheric extrusion into the middle and lower troposphere may have been an important source of vorticity for the cyclone, which began to develop downstream of the fold within the following 12 h.

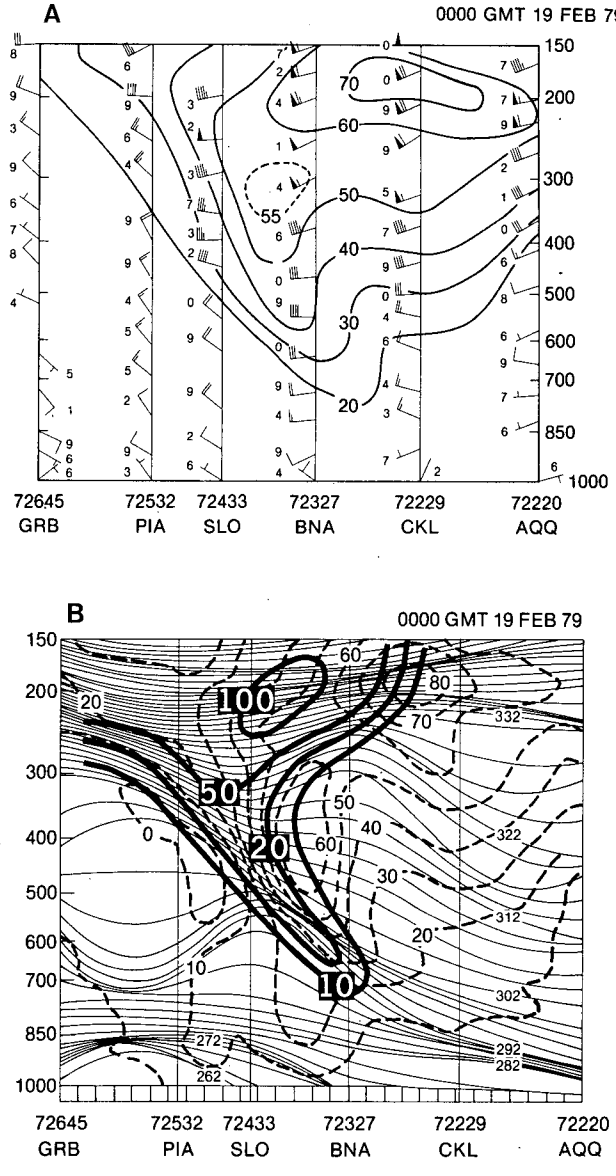

FIG. 6. Vertical cross section from Green Bay, Wisconsin (GRB), to Apalachicola, Florida (AQQ), for 0000 GMT 19 February 1979. (A) Isotach analysis for total wind speed (solid, m s^{-1}); wind barbs plotted with last digit of wind observation. (B) Isentropes (solid, K), geostrophic wind (dashed, m s^{-1}) computed from the horizontal thermal gradient in the plane of cross section, and potential vorticity, $-(\zeta_\theta + f)(\partial\theta/\partial p)$, (dark solid where $10 = 10 \times 10^{-6}$ K s^{-1} mb^{-1}). Potential vorticity analysis only shown for upper portion of frontal zone and stratosphere.

By 12Z/19, rapid cyclogenesis was in progress along the Virginia coast with heavy snow occurring from northern Virginia to extreme southeastern New York (Fig. 1E). Bosart's (1981) analysis shows that the coastal front was still present in eastern Maryland, providing the low-level convergence that enhanced snowfall rates

from Washington, D.C., northward toward New York City. The isentropic analyses for 12Z/19 (Fig. 7) show that the PJ–trough system propagated eastward from the Ohio Valley to the East Coast without noticeable amplification of the trough in the middle and upper troposphere as the cyclogenesis commenced offshore. The LLJ, which developed south of the STJ at 12Z/18 (Fig. 4C1) and moved slowly up the East Coast by 00Z/19 (Fig. 5C1), had now become incorporated within the circulation of the cyclone by 12Z/19 (Fig. 7C1). The LLJ was directed up the 292 K isentropic surface and appeared to be transporting moisture into the region of heavy snowfall for the third consecutive observing period. The cyclone subsequently developed

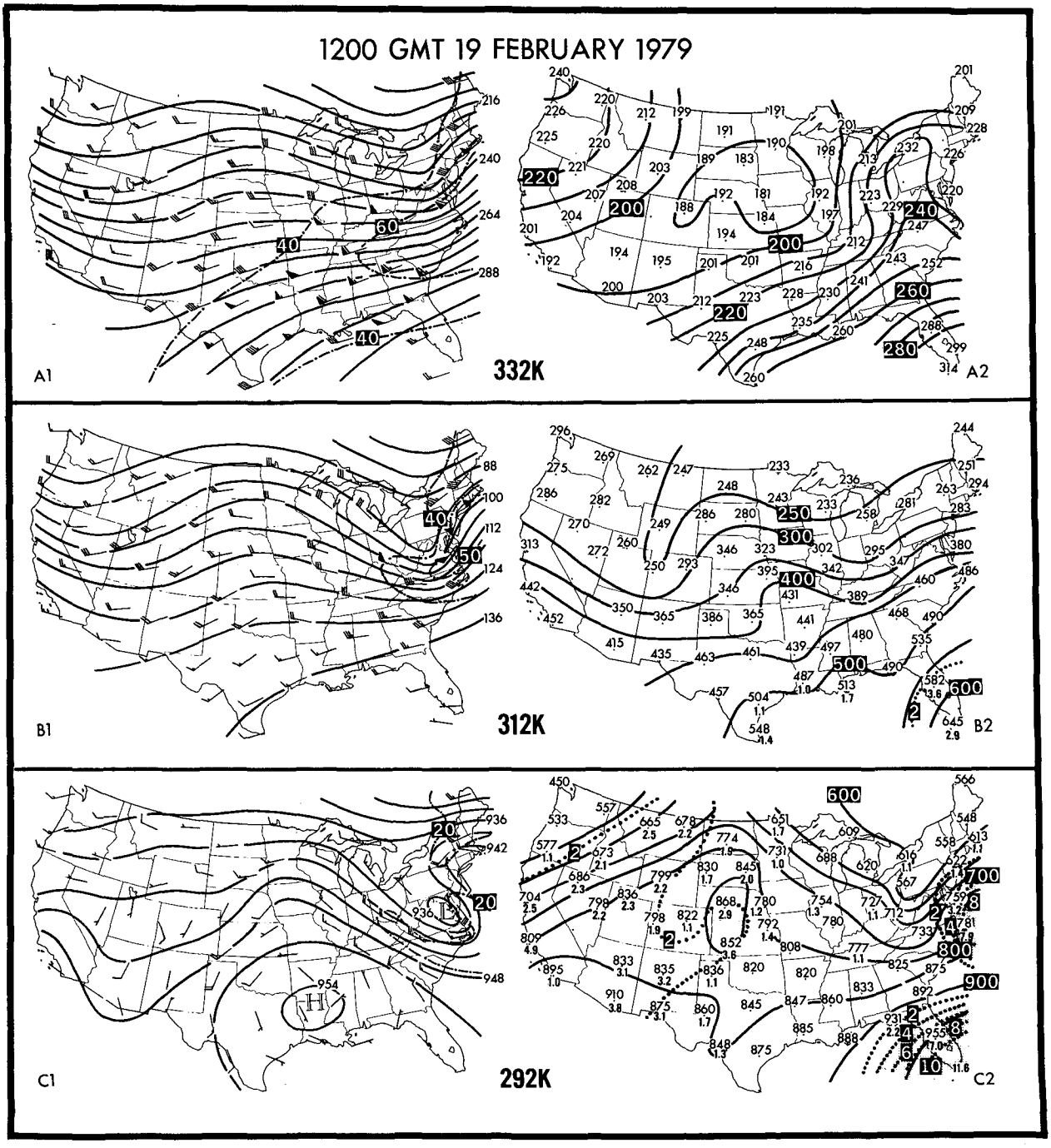

FIG. 7. As in Fig. 2 but for 1200 GMT 19 February 1979.

into a major vortex and moved eastward in the next 12 h (Fig. 1F).

b. SMS-GOES infrared imagery

SMS-GOES infrared imagery (Fig. 8) depicts two separate cloud regimes associated with the heavy snows on 18 and 19 February. The first of these areas appears as an extensive cloud shield over the eastern United States at 12Z/18 (area S on Fig. 8), which coincides with the position of the STJ. The heavy snow in Tennessee, the Carolinas and southern Virginia was not located under the coldest cirrus cloud tops, but along the southern edge of the cloud domain. This is a common feature based upon our observations through several winter seasons and agrees with results recently presented by Scofield *et al.* (1982) and Browning (1983). Between 12Z/18 and 12Z/19, the area of high clouds drifted eastward and decreased in size (especially after 00Z/19). The distribution of clouds over the eastern United States seems to be correlated with the position and movement of the various jet streaks. The area of high clouds centered over West Virginia at 12Z/18 (Fig. 8A) corresponds with the region in which the STJ extended from 240 to approximately 200 mb, as inferred from the airflow along the sloping 332 K isentropic surface (Fig. 4A2). The lack of clouds over the New England states through 18Z/18 was associated with the descent of the polar jet located along the Northeast Coast from 300 to 340 mb as inferred from the airflow along the sloping 312 K surface (Fig. 4B2).

A second, less distinct area of clouds displaying a vortical form was located over the north-central United States at 12Z/18 (area P on Fig. 8). These clouds are evidence of rising motions within and ahead of the trough moving across the Midwest. By 2330Z/18, the cloud area was located within the exit region of the PJ and immediately downstream of the trough axis (Fig. 5B1) and tropopause fold (Fig. 7B). The cloud area rapidly expanded and deepened (i.e., cloud top temperature decreased significantly) as it moved towards the East Coast between 00Z/19 and 12Z/19. The explosive growth was accompanied by heavy snowfalls initially in western Pennsylvania, and later along the East Coast. Again, the heaviest snow occurred within the southern edge of the cloud domain as the cirrus shield expanded toward southern New England.

Hourly infrared images (not shown) reveal that the rapid intensification and expansion of the second cloud area coincided with the vigorous cyclogenesis[2] off the North Carolina–Virginia coast prior to 12Z/19 as the PJ-trough system propagated rapidly eastward from the Ohio Valley. The region of maximum pressure falls observed from 00Z/19 to 12Z/19 was located along the North Carolina–Virginia coast (see Fig. 4 in Bosart, 1981), immediately to the west of the cirrus shield associated with the STJ, in an area of shallow (warmer) cloud cover where convective clouds were not apparent.

The infrared imagery (Fig. 8F) also illustrates the rapid evolution and highly asymmetrical nature of the cloud distribution associated with rapid cyclogenesis between 12Z/19 and 18Z/19 as the cloud mass moved eastward and became more nearly colocated with the deepening surface cyclone. It was not until 1130 GMT 19 February that the convective cells defined by Bosart's analysis (C on Figs. 8E and F) developed immediately to the south of the vortex center (Fig. 8E). The cell intensity appears to diminish after 1230 GMT as the cloud top temperatures increased and the areal extent of the individual convective cells decreased by 1800 GMT (Fig. 8F). The infrared imagery suggests that the influence of these convective cells in the total evolution of the cyclone was small even though they developed simultaneously with the onset of rapid deepening near 12Z/19. However, the diabatic processes associated with the widespread precipitation within the rapidly expanding cloud mass over the Mid-Atlantic States, to the north of the cyclone center at 12Z/19, may well have played an important role in enhancing cyclogenesis during its initial stages.

3. Analysis of jet streaks prior to cyclogenesis

The synoptic overview of the Presidents' Day cyclone identified three distinct intensifying jet streaks that appear to have influenced the rapid cyclogenesis and the development of the heavy snowfall. Wind speeds along the axis of the STJ increased during the 24 h period ending 12Z/18 as the first area of moderate to heavy snow developed in the southeastern United States. Simultaneously, an intense LLJ rapidly developed south of the axis of the STJ, increasing the warm air advection near the 850 mb level along the coast (Bosart, 1981). The intense and rapid cyclogenesis occurred after the PJ–trough system intensified over the central United States and then approached the thermal ridge along the coast.

The infrared imagery supports the hypothesis that the rapid cyclogenesis along the Carolina–Virginia coast after 06Z/19 was linked, in part, to an interaction among the various jet streaks. As has been discussed by Petterssen (1956) for other cyclones, the relative movements of the upper- and lower-tropospheric systems (where a lower-tropospheric thermal field was geographically bounded while it was overtaken by a rapidly advancing PJ–trough system) were important elements for the rapid cyclogenesis on 19 February 1979. The increased thermal and moisture advections associated with the LLJ and subsequent coastal frontogenesis made the region more conducive to cyclogenesis by enhancing the low-level thermal ridge and

[2] The central pressure of the storm decreased at a rate of more than 1 mb h^{-1} during this period.

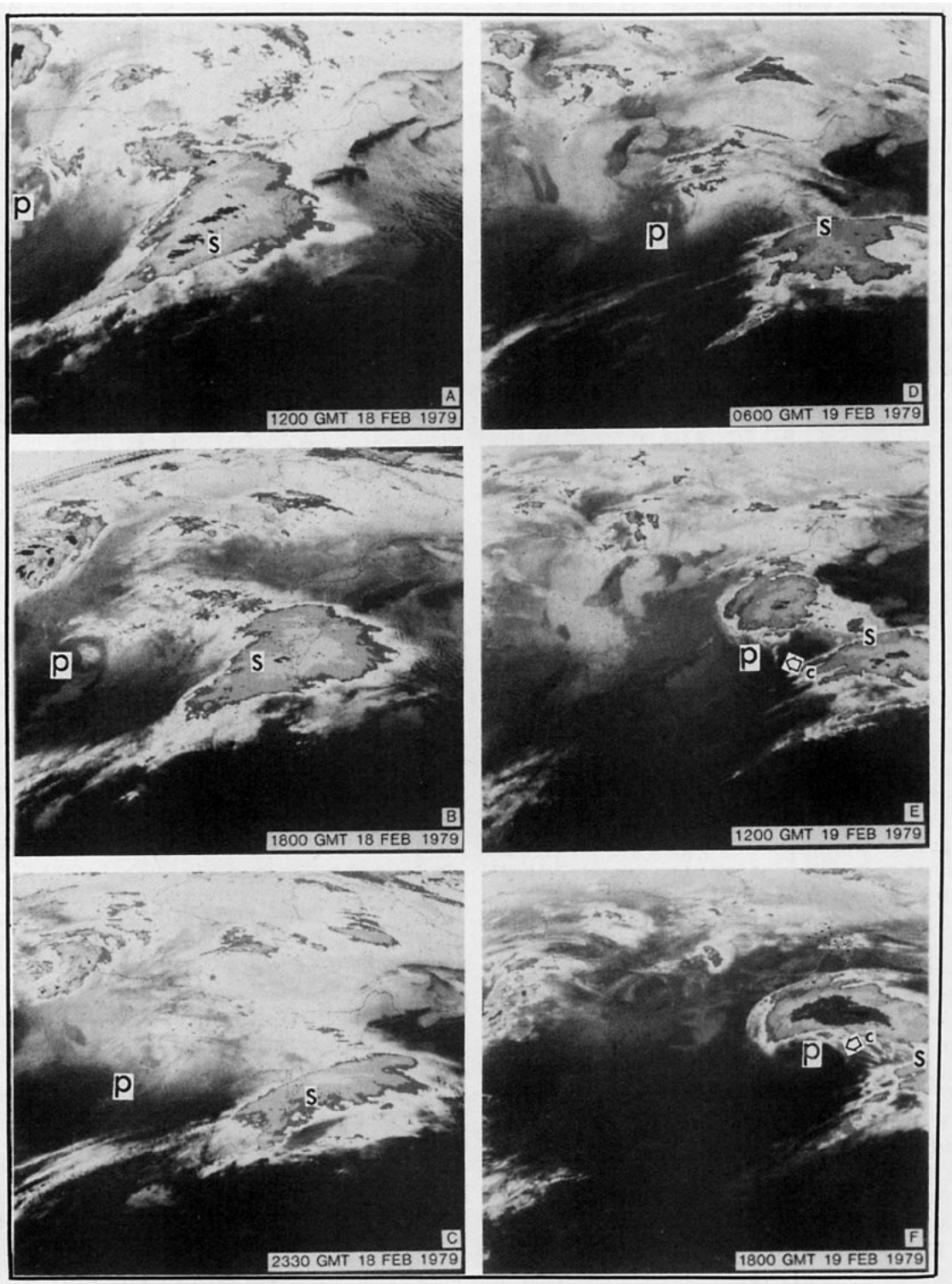

FIG. 8. Six-hourly SMS–GOES infrared satellite imagery prior to and during cyclogenesis: (A) 1200 GMT 18 February 1979, (B) 1800 GMT 18 February 1979, (C) 2330 GMT 18 February 1979, (D) 0600 GMT 19 February 1979, (E) 1200 GMT 19 February 1979, and (F) 1800 GMT 19 February 1979. S and P represent positions of maximum winds associated with the subtropical and polar jet streaks, respectively. C represents position of convective cells to the south of the developing cyclone.

inverted trough immediately along the East Coast. The cloud area associated with the PJ–trough then expanded rapidly and vigorous cyclogenesis commenced as the PJ and trough propagated eastward and encountered the northern extent of the inverted trough which had developed along the coast by 00Z/19.

The following diagnostic analysis focuses on the STJ with future work directed toward a detailed analysis of the LLJ and PJ–trough system. The diagnostic study includes: (1) an analysis of the total, geostrophic and ageostrophic wind fields, (2) a trajectory analysis, (3) an evaluation of the ageostrophic flow based on the geostrophic momentum approximation, and (4) an analysis of the upper-level divergence. The diagnostics are chosen to identify processes responsible for the enhancement of the STJ prior to 12Z/18 and to present evidence suggesting that the STJ was becoming increasingly unbalanced as it amplified. While systematic errors in either the wind or mass fields and missing wind reports in the data set could adversely affect the diagnostic computations, the large areal extent and the coherent temporal evolution of the fields examined in this section indicate that neither systematic errors nor data gaps were large enough to obscure significant features in the following analyses.

a. Examination of the geostrophic and ageostrophic components associated with the STJ

Many authors, including Bjerknes (1951), Murray and Daniels (1953), Newton (1959), Uccellini and Johnson (1979) and Shapiro and Kennedy (1981), have described the orientation of the ageostrophic flow in the entrance and exit regions of finite-length, straight jet streaks, summarized in Newton's (1959) schematic (Fig. 9). Fig. 9 illustrates these features for an assumed symmetrical jet streak that preserves its shape with time. In the following discussion, favorable comparisons with the schematic are noted when applicable. We then emphasize the important departures from the idealized schematic for a situation wherein the configuration of the flow pattern changes with time and the accelerations differ fundamentally from those in Fig. 9. Accordingly, the divergence pattern associated with the ageostrophic wind field is also different, with important implications for the development of heavy snow along the axis of the STJ, as will be shown in Section 4. In the entrance region of the idealized jet streak, the ageostrophic component is directed toward the cyclonic side of the jet and can be related to the confluence in the stream function and along-stream increase in the wind speed (Namias and Clapp, 1949). The cross-stream ageostrophic flow in the entrance region represents the upper branch of a direct transverse circulation that converts available potential energy into kinetic energy for parcels accelerating into the jet. In the exit region of the jet, the ageostrophic components are directed toward the anticyclonic side. This ageostrophic cross-contour flow represents the upper branch of an indirect transverse circulation that converts kinetic energy to available potential energy as parcels decelerate upon exiting the jet.

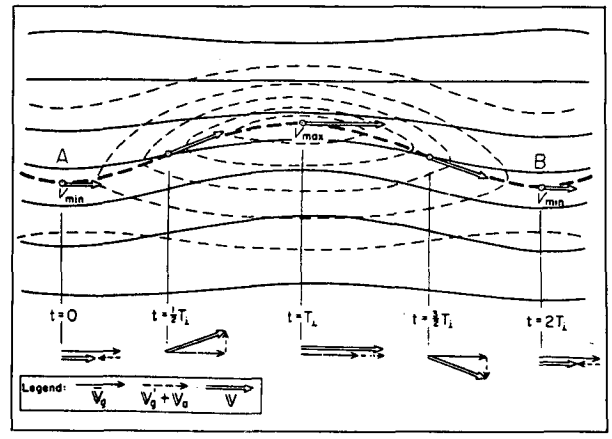

FIG. 9. Schematic contours (solid), isotach (thin dashed) and vector winds illustrating an ageostrophic oscillation for an air parcel propagating through a jet streak (from Newton, 1959).

To illustrate the structure and temporal evolution of the total, geostrophic and ageostrophic wind fields associated with the STJ, streamline and isotach analyses on the 332 K surface are shown in Fig. 10. The total wind speed maximum along the axis of the STJ increased from around 65 m s^{-1} at 12Z/17 to nearly 75 m s^{-1} at 00Z/18 to greater than 80 m s^{-1} by 12Z/18 as the STJ propagated toward the East Coast (Fig. 10A). The wind speeds increased as the distance between the trough and ridge lines (Fig. 10B) decreased by 400 km along the axis of the STJ between 00Z/18 and 12Z/18 (since the trough propagated eastward at nearly 20 m s^{-1} while the ridge propagated eastward at $\sim$10 m s^{-1}). While the total wind maximum increased by more than 15 m s^{-1} in the 24 h ending at 12Z/18, the geostrophic wind maximum (Fig. 10B) increased from 55 m s^{-1} to 58 m s^{-1} to only 63 m s^{-1} during the same period and consistently lagged the position of the total wind maximum. By 12Z/18, the maximum geostrophic wind was displaced nearly 700 km to the southwest of the jet core (indicated by a J in Fig. 10A). This displacement, combined with the increase in the total wind speed, resulted in an increase in the ageostrophic wind speed to a magnitude greater than 30 m s^{-1} near the core of the STJ by 12Z/18.

Several aspects of the ageostrophic winds associated with the STJ (Fig. 10C) favorably agree with Newton's idealized schematic (Fig. 9). For example, the ageostrophic winds in the entrance region of the STJ were directed toward lower ψ_m values in western Texas at 12Z/17, then from Texas to Missouri at 00Z/18, and finally from Louisiana through Missouri by 12Z/18, indicating the presence of a direct circulation. Along the axis of the STJ and near the jet core, the 20 m s^{-1}

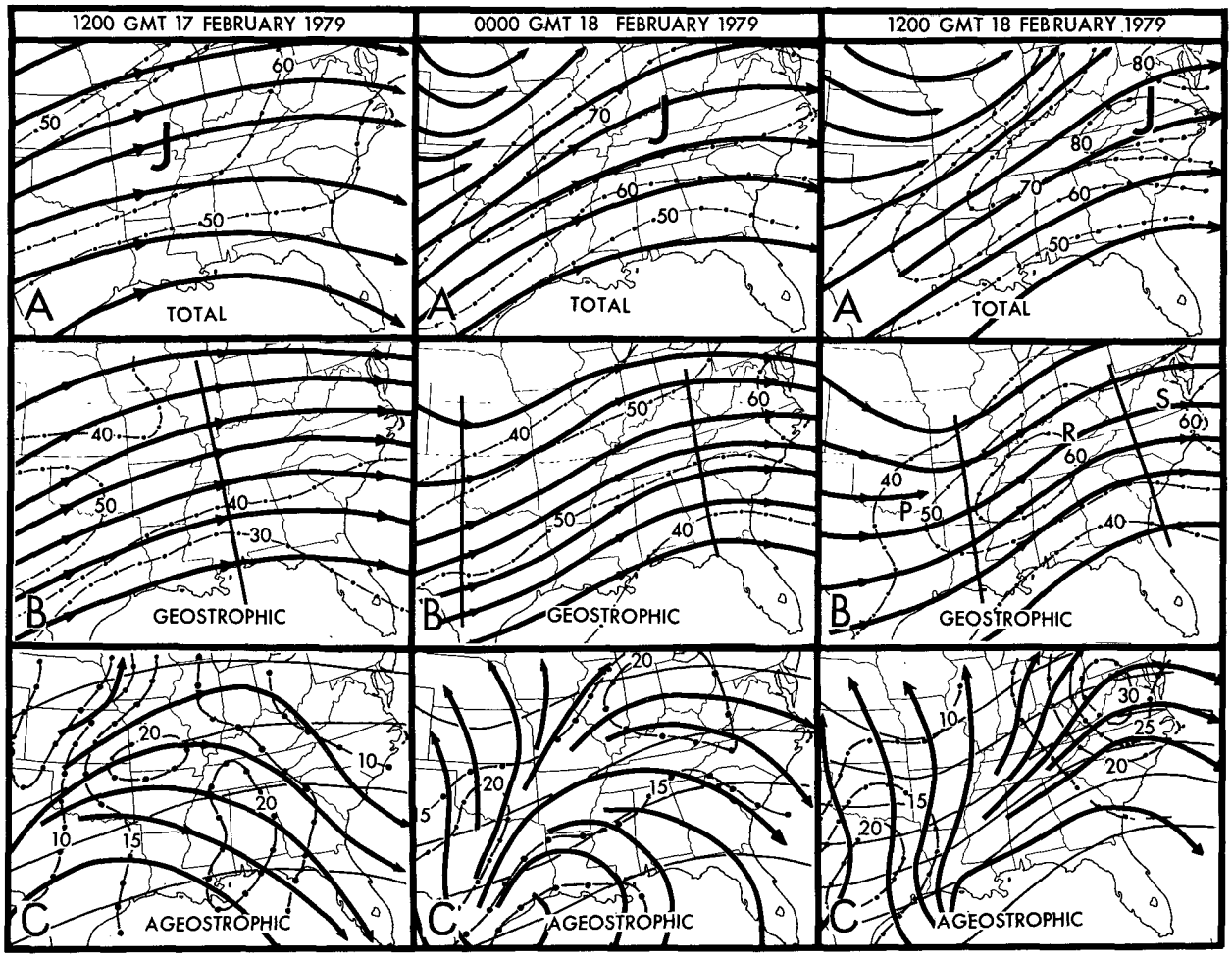

FIG. 10. (A) Total, (B) geostrophic, and (C) ageostrophic winds for 332 K at 1200 GMT 17 February, 0000 GMT and 1200 GMT 18 February 1979, including streamlines (thick solid) and isotachs (dot-dash, m s^{-1}). In (A), *J* represents position of maximum winds associated with the STJ. In (B), straight solid lines oriented north–south represent trough and ridge axes. P, R, S (at 1200 GMT 18 February) are points chosen for the evaluation of the geostrophic momentum approximation (Table 2). In (C), thin solid lines represent contours of constant ψ_m.

ageostrophic winds were primarily in the along-stream direction at 12Z/17 and 00Z/18. In the exit region of the STJ, the ageostrophic components were directed toward higher ψ_m values over the southeastern United States at 12Z/17 and 00Z/18 and over to the East Coast by 12Z/18 (Fig. 10C), indicating the presence of an indirect circulation.

At 12Z/18, several changes in the ageostrophic wind field became evident. *Within the entrance region* of the STJ, which extended from the Texas–Mexico border to southwestern Virginia, there were *two distinct* areas in which the ageostrophic wind had a *significant* component directed toward lower ψ_m, where only one area was evident at previous times. The first area was located from Texas to Missouri in the confluent portion of the entrance region, while the second new area was located from Tennessee to West Virginia immediately upstream of the ridge axis. The two areas of ageostrophic flow directed toward lower ψ_m in the entrance region of the STJ as well as the large displacement between the geostrophic and total wind maxima represent significant departures from Newton's schematic (Fig. 9).

A trajectory analysis is presented next to provide additional evidence for the existence of two regions of cross-contour ageostrophic flow in the entrance region of the STJ. Trajectories were computed on the 332 K surface during the two 12 h periods between 12Z/17 and 12Z/18 using a discrete model approach (Petersen and Uccellini, 1979) that explicitly relates ageostrophic flow to parcel accelerations in an energy conserving manner. Initial and final ψ_m values used in the trajectory computations were derived from the objective analysis, while station wind reports were used to initialize the trajectories. The limitations of the trajectory approach and a discussion of a technique to simulate

the movement of identifiable features in the ψ_m analysis between observation times are presented in the Appendix. The explicit approach for deriving trajectories represents an attempt to compute the response of a parcel to changing pressure gradient and Coriolis forces in a nearly continuous manner. The parcel velocity is constrained only by the frictionless, adiabatic equation of motion. Given these assumptions and other deficiencies in the trajectory method listed in the Appendix, a perfect match between the final parcel velocity and the actual wind analysis should not be expected. Yet, the trajectory computations provide another measure of the ageostrophic wind vectors during a 12 h period which support the analyses of the ageostrophic winds along the STJ axis (Fig. 10).

Several trajectories representative of the flow through the STJ between 12Z/17 and 12Z/18 are superimposed on the ψ_m analysis in Fig. 11. During both time periods, the southernmost trajectories that remained on the anticyclonic side of the STJ (parcels 5 and 10) accelerated toward lower ψ_m values, passed to the south of the jet core, then turned toward higher ψ_m values and decelerated, in agreement with Newton's schematic (Fig. 9). In contrast, the trajectories that passed through the STJ maximum (parcels 1–3, 7–9) generally underwent two periods of acceleration. The first acceleration occurred over Texas as the parcels entered the STJ. Upon exiting the region of maximum pressure gradient near Arkansas and Tennessee, the parcels ceased accelerating for a short period, then accelerated again from eastern Kentucky to Virginia and were again directed toward lower ψ_m values. Fig. 11 also shows that the parcel accelerations over Texas between 00Z/18 and 12Z/18 were larger than the accelerations between 12Z/17 and 00Z/18. The increased acceleration into the STJ during the 00Z/18 to 12Z/18 period is consistent with the increased magnitude of the cross-stream ageostrophic wind over Texas by 00Z/18 (Fig. 10C) and the developing confluence in the streamlines of the geostrophic wind (Fig. 10B). The increased confluence in this region at 12Z/18 appears to be associated with an interaction between the PJ and STJ, as the PJ–trough system continually propagated toward the entrance region of the STJ between 12Z/17 and 00Z/19 (Figs. 2–5). The net result is that parcels propagating along the axis of the STJ toward the ridge axis had greater wind speeds between 00Z/18 and 12Z/18 than during the previous 12 h.

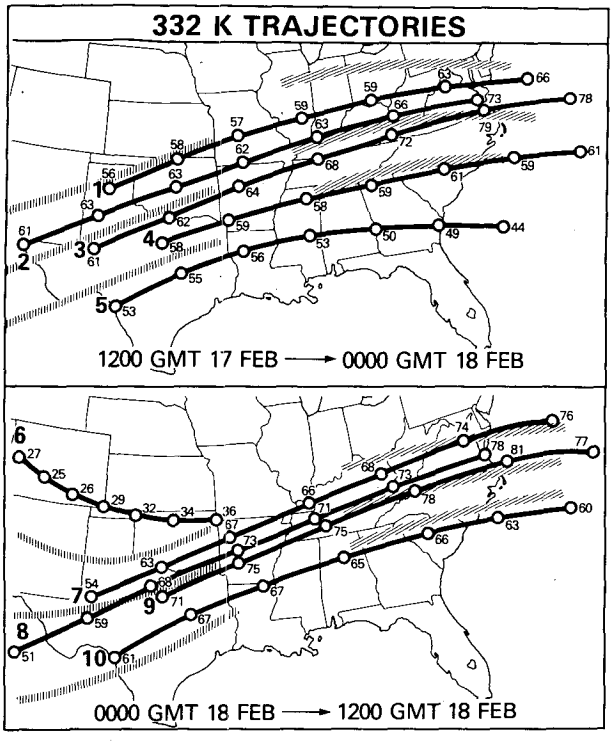

FIG. 11. 332 K trajectories initialized at 1200 GMT 17 February (top) and 0000 GMT 18 February 1979 (bottom). Figure includes parcel locations and speeds (m s^{-1}) at 2 h intervals. Vertically hatched and shaded thick lines represent analyses of ψ_m at beginning and end of 12 h period used in trajectory computations.

The decomposition of the total wind into its geostrophic and ageostrophic components for parcel 8, which is considered typical of parcels passing through the STJ between 00Z/18 and 12Z/18, is depicted at 2 h intervals in Fig. 12 and listed at half-hour intervals in Table 1. The wind speeds and directions along the entire trajectory appear to represent the wind observations along the axis of the STJ fairly well for this period, with the final wind speed and direction of the parcel being within several m s^{-1} and 10° of the analyzed wind at 12Z/18 (Fig. 4A1). Table 1 and Fig. 12 show that the initial accelerations for parcels entering the STJ were associated with 20 m s^{-1} ageostrophic wind components directed from the south toward lower ψ_m values on the cyclonic side of the jet. Parcel 8 was initially subgeostrophic, but the southerly ageostrophic winds between 15 to 20 m s^{-1} were maintained at a significant angle to the geostrophic wind for the first 4.0 h of the trajectory. The parcel, therefore, accelerated towards lower ψ_m values in the entrance region of the STJ, became significantly supergeostrophic within 2 h, and increased in speed by 22 m s^{-1} by 6 h. While only a 2 h period was required for it to become supergeostrophic, the parcel needed 6 h to attain a geostrophic direction through inertial rotation. The existence of a 12 m s^{-1} supergeostrophic flow parallel to the geostrophic streamlines at 6 h (Table 1) is a consequence of the continual adjustment of the parcel velocity to an increasing pressure gradient force as the parcel moved into the entrance region of a finite-length jet.

After the parcel achieved a "directional" balance, the acceleration ceased between hours 6.0 and 8.5 (Table 1) as the parcel direction veered due to inertial rotation and the geostrophic wind direction changed from 250° and 256° at approximately the same rate.

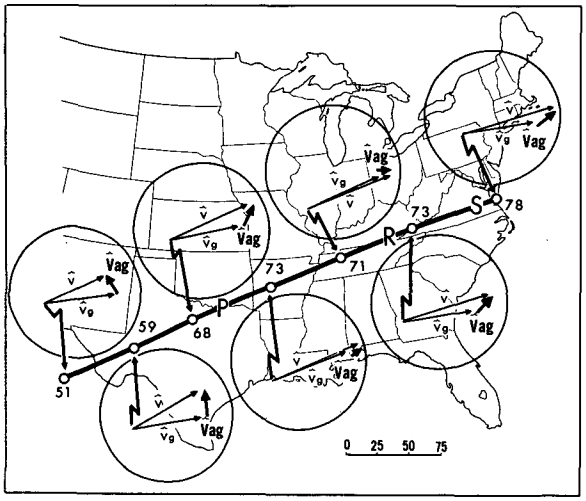

FIG. 12. Total, geostrophic and ageostrophic vectors at 2 h intervals for trajectory 8 in Fig. 11 initialized at 0000 GMT 18 February 1979 on 332 K surface. Vector scale (m s^{-1}) is located at the bottom of the figure. P, R, S are points chosen for evaluation of the geostrophic momentum approximation (Table 2).

At hour 9.0, a second acceleration commenced as the parcel moved toward the ridge axis over the eastern United States. As the parcel approached the ridge between hours 9.0 and 11.5, the direction of the pressure gradient force veered rapidly and its magnitude weakened (see Table 1). Since the parcel had an ageostrophic component in the direction of the total wind as it approached the ridge, the parcel continued to turn toward the right of its instantaneous motion due to inertial rotation. Nevertheless, a combination of 1) the decreasing distance between the confluence zone in the entrance region of the STJ (where the parcel first accelerated) and the ridge axis (Fig. 10B) and 2) the parcel's high wind speed did not allow enough time for the Coriolis acceleration to turn the parcel to the right as quickly as the geostrophic wind veered. As a result, the parcel again was directed toward lower ψ_m values with a southwesterly ageostrophic component greater than 20 m s^{-1}. The parcel, therefore, accelerated through the ridge rather than following the ψ_m contours around the ridge crest or turning toward higher ψ_m values. This portion of the trajectory, with an ageostrophic component directed toward the cyclonic side of the jet near the ridge crest, differs from Newton's schematic (Fig. 9). This difference is related, in part, to the dissimilarities in the location of the strongest ψ_m gradient between the real and idealized cases. In this case, the strongest ψ_m gradients were located on either side of the ridge crest, rather than near the jet core as in Newton's schematic, with a weaker ψ_m gradient in the region of maximum winds near the ridge axis.

In summary, the trajectories along the axis of the STJ underwent two periods of acceleration and provide

TABLE 1. Data tabulation for parcel trajectory 8 (Fig. 12) computed on the 332 K surface between 00Z/18 and 12Z/18.

				Total wind		Geostrophic wind		Ageostrophic wind	
Time (h)	Pressure (mb)	Latitude (deg)	Longitude (deg)	Direction (deg)	Speed (m s^{-1})	Direction (deg)	Speed (m s^{-1})	Direction (deg)	Speed (m s^{-1})
0.0	239.8	28.69	106.06	235.0	51.0	253.6	53.9	141.7	17.3
0.5	236.1	29.17	105.27	235.0	53.0	250.3	54.3	147.9	14.3
1.0	233.6	29.67	104.45	235.2	54.8	249.6	54.4	153.8	13.7
1.5	232.1	30.19	103.59	235.6	56.6	252.4	54.2	162.3	16.4
2.0	231.2	30.71	102.69	236.4	58.9	256.6	54.2	169.6	20.3
2.5	230.9	31.24	101.74	237.6	61.5	258.9	54.3	176.7	22.6
3.0	231.7	31.77	100.72	239.2	64.2	258.7	53.8	186.0	22.5
3.5	233.4	32.30	99.64	240.9	66.5	257.3	53.3	196.6	21.4
4.0	234.7	32.81	98.50	242.9	68.4	256.5	53.7	205.0	20.6
4.5	234.5	33.31	97.29	244.8	70.1	255.9	55.1	211.3	19.2
5.0	233.4	33.78	96.04	245.6	71.4	254.8	57.4	217.4	16.7
5.5	231.5	34.23	94.74	248.2	72.5	253.2	59.7	226.5	14.0
6.0	230.3	34.65	93.41	249.7	72.9	250.7	61.1	244.4	11.9
6.5	227.7	35.05	92.05	251.0	72.8	248.9	61.9	262.7	11.2
7.0	222.8	35.42	90.69	252.3	72.3	248.6	62.2	273.2	10.9
7.5	217.1	35.76	89.32	253.5	71.7	250.2	61.9	273.4	10.5
8.0	211.8	36.08	87.94	254.7	71.2	252.7	60.9	266.0	10.6
8.5	207.6	36.37	86.56	256.0	71.0	256.0	59.2	256.1	11.8
9.0	204.2	36.63	85.17	257.6	71.2	260.0	57.5	247.6	14.0
9.5	201.7	36.86	83.75	259.5	71.8	264.8	55.3	242.7	17.5
10.0	200.6	37.05	82.31	261.8	72.8	270.2	53.1	241.0	21.7
10.5	201.6	37.20	80.82	264.6	74.2	273.4	51.0	246.3	25.1
11.0	204.4	37.28	79.31	267.6	75.3	275.2	51.3	251.9	25.4
11.5	208.3	37.30	77.76	270.4	76.4	278.8	53.9	251.7	24.4
12.0	213.6	37.26	76.19	273.0	77.7	279.5	57.9	255.1	21.2

additional evidence for the presence of the two areas in which an ageostrophic wind component was diagnosed to be greater than 20 m s^{-1} and directed toward lower ψ_m values at a significant angle to the geostrophic streamlines in the entrance region of the STJ (Fig. 10C). It appears that two major factors contributed to the double acceleration experienced by parcels passing through the STJ, yielding the supergeostrophic, cross-stream flow toward lower ψ_m values upstream of the ridge crest. The first was the increasing confluence in the entrance region of the STJ between 12Z/17 and 12Z/18. The second was the decreasing distance between a trough propagating through the Central Plains and a more slowly moving ridge over the eastern United States. The parcels accelerated into the STJ, attained a high wind speed and then rapidly encountered a ridge with insufficient time for inertial rotation and were again directed toward lower ψ_m. Therefore, parcels which passed through the STJ underwent a second period of acceleration and became increasingly supergeostrophic at the ridge crest.

b. *Evidence for unbalanced flow along the axis of the STJ*

The analyses of the geostrophic and ageostrophic winds (Fig. 10) reveal that the winds in the STJ became increasingly supergeostrophic between 12Z/17 and 12Z/18 as the jet streak propagated towards the East Coast. In addition, two distinct maxima of cross-contour ageostrophic wind components developed within the entrance region. The placement of the maximum ageostrophic wind speed near the ridge axis at 00Z/18 and 12Z/18 (Fig. 10C) agrees with the concept of an anticyclonic jet in gradient balance (e.g., Endlich and McLean, 1960). The extent to which gradient balance accounts for the maximum winds associated with the STJ near the ridge crest is difficult to assess given the uncertainties of gradient wind computations near ridges (Petterssen, 1956, p. 65; Haltiner and Martin, 1957, pp. 189–190; Newton and Persson, 1962), the limitations of the trajectory scheme (Appendix A), and the general difficulty of computing a radius of trajectory curvature for nonsteady situations (Endlich, 1961). *Nevertheless, at 12Z/18 the ageostrophic winds have a large component directed toward lower ψ_m values, indicating that the total wind was neither in geostrophic nor gradient balance within a significant portion of the STJ.*

The analysis of the STJ in Fig. 10 is consistent with Bjerknes' (1954) discussion of unbalanced accelerating flow at a ridge crest, which can develop when the wavelength between an upstream trough and ridge decreases. Bjerknes defined a critical radius of streamline curvature (R_c) as a criterion for unbalanced flow at a ridge. At 12Z/18, when the total wind speed of the STJ was nearly 1.5 times larger than U_g, R_c is defined by the expression

$$R_c = \frac{1.5(1.5U_g - c)}{\Omega \sin\phi}, \quad (1)$$

where c is the propagation rate of the ridge and Ω is the angular velocity of the Earth's rotation. If R_c is larger than the actual radius of curvature of the ψ_m field, the streamlines will be at a significant angle to the ψ_m contours and gradient balance is not possible (Bjerknes, 1954, p. 45). At 12Z/18, R_c was 2.4×10^3 km, U_g was 53 m s^{-1}, c was 9 m s^{-1} and ϕ was 38°. Since the actual radius of curvature of the 332 K ψ_m field at the ridge crest was measured[3] as less than 2.0×10^3 km, the supergeostrophic flow was unbalanced by Bjerknes' criterion and parcels approaching the ridge axis should be expected to accelerate toward lower ψ_m values. This result agrees with Newton's (1981) contention that nongradient flow in a STJ is significant when the wavelength of a trough–ridge system is short compared to the climatological structure of the STJ associated with the planetary long-wave pattern.

Another criterion for determining if the STJ was unbalanced is whether the divergence tendency following a parcel is large enough for the assumptions made in the derivation of the nonlinear balance equation to break down. In their evaluation of the divergence equation, House (1961), Paine *et al.* (1975), and Kaplan and Paine (1977) noted that when a jet streak approaches a ridge, the upper-level divergence can increase significantly due to the dominance of the Jacobian and Laplacian terms. Moreover, parcels moving through the jet would experience such a large increase in divergence that the balance equation becomes inapplicable. Van Tuyl and Young (1982) conducted a channel model simulation of a straight jet streak and characterize the temporal increases of divergence along the jet axis to be symptomatic of unbalanced flow which cannot be accounted for by either the quasi-geostrophic or the balance equations.

To compute the divergence for this case, the gridded winds on isentropic surfaces were vertically interpolated to pressure surfaces at 25 mb intervals. The divergence fields are shown in Fig. 13 for the 225 mb surface, which represents an average pressure level along the axis of the STJ at 12Z/17, 00Z/18, 12Z/18 (Figs. 2A2, 3A2, and 4A2). The divergence patterns at 200 mb and 250 mb (not shown) have the same general pattern and temporal evolution. Fig. 13 depicts a general tendency for a four-cell pattern of divergence expected near a straight-line jet streak, especially at 00Z/18, with divergence in the left front and right rear quadrants and convergence in the right front and left rear quadrants (Riehl *et al.*, 1952; Beebe and Bates, 1955). The curvature effects associated with the anticyclonic flow

[3] The radius of curvature of the ψ_m field was determined by computing the change of direction of the geostrophic wind along the geostrophic streamlines and correcting for earth curvature (Platzman, 1947).

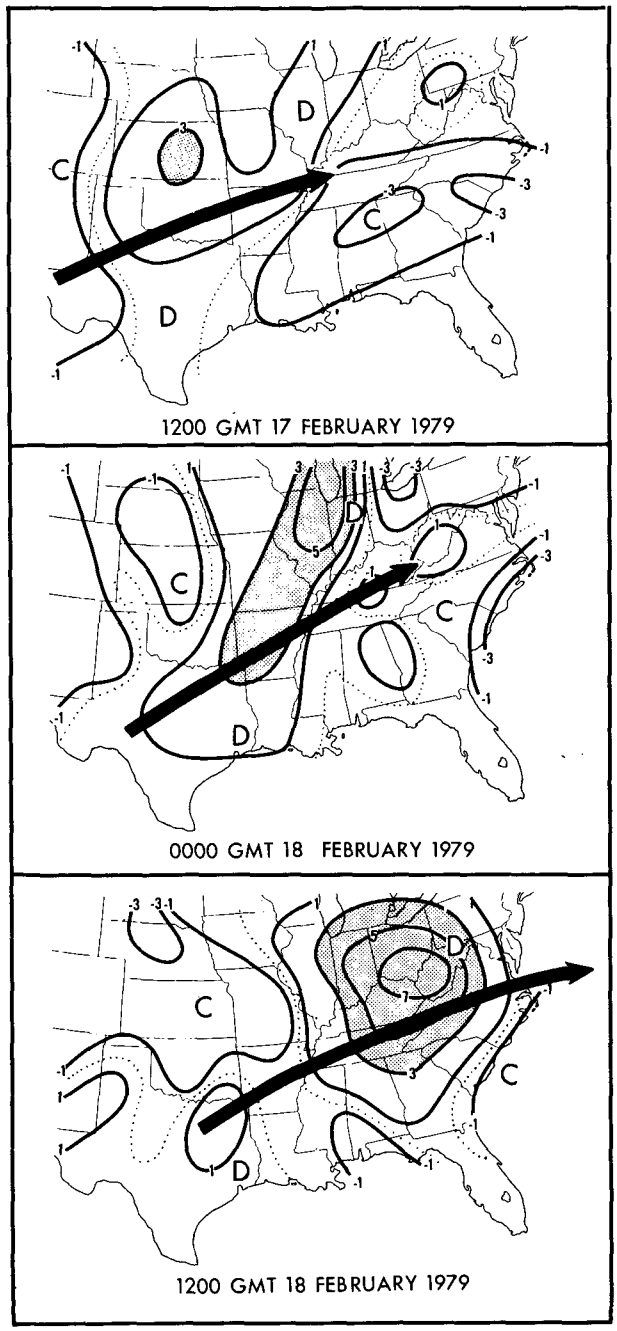

FIG. 13. Divergence ($5 = 5.0 \times 10^{-5}$ s^{-1}) for 225 mb pressure surface for 1200 GMT 17 February, 0000 GMT 18 February, and 1200 GMT 18 February 1979. See text for method of computation. Solid line indicates position of axis of the subtropical jet streak and shaded area is divergence larger than 3.0×10^{-5} s^{-1}.

appears to have influenced the divergence field since the maximum divergence in Kansas (12Z/17), Illinois (00Z/18), and West Virginia (12Z/18) was located immediately upstream of the ageostrophic wind maximum near the ridge position (Fig. 10). However, there is a tendency for the divergence to increase with time between 12Z/17 and 12Z/18 in conjunction with the previously noted increase in the cross-contour ageostrophic flow (Fig. 10C), especially along the axis of the STJ over Tennessee and Virginia between 00Z/18 and 12Z/18. With the 12 h separation between observing times, it is impossible to determine if the 7×10^{-5} s^{-1} divergence maximum at 12Z/18 represents a local increase of the divergence that was over West Virginia at 00Z/18 or an amplification of the divergence field that was over Illinois at 00Z/18 as it propagated eastward.[4] Nevertheless, during the 4 h needed for parcels to propagate along the axis of the STJ from Arkansas to West Virginia around 12Z/18 (Fig. 11), the parcels would experience an increase in divergence in excess of 4×10^{-9} s^{-2}. This value for $d(\nabla \cdot \mathbf{U})/dt$ is as large as the magnitude for individual terms in the divergence equation at the subsynoptic to synoptic scale (Kaplan and Paine, 1977). Therefore, the assumption needed to derive the balance equation (i.e., $d(\nabla \cdot \mathbf{U})/dt$ is negligible) would not be satisfied for this case even on the coarse 2° by 2° latitude–longitude grid used in this diagnostic analysis.

The large increase of divergence associated with the developing cross-contour ageostrophic winds as the STJ propagated toward the ridge axis is similar to the analyses of House (1961), Paine *et al.* (1975), and Kaplan and Paine (1975), and is also consistent with Van Tuyl and Young's (1982) designation of unbalanced jet flows which are not properly described by either quasi-geostrophic theory or the balance equation. These findings, combined with the earlier discussion of the nongradient aspects of the STJ in accordance with Bjerknes (1954) and Newton (1981), all provide evidence that the STJ was becoming increasingly unbalanced between 12Z/17 and 12Z/18.

c. Evaluation of the geostrophic momentum approximation

The trajectory analysis provided a means to resolve the processes that contributed to the parcel accelerations along the axis of the STJ. The purpose of this subsection is to determine if the geostrophic momentum approximation to the parcel acceleration can account for the two distinct periods of parcel acceleration that contributed to the supergeostrophic flow near the jet core. The geostrophic momentum approximation (Eliassen, 1948) applied to the frictionless, adiabatic equation of motion in isentropic coordinates,

$$\frac{d\mathbf{U}}{dt} = \left(\frac{\partial \mathbf{U}}{\partial t} + \mathbf{U} \cdot \nabla_\theta \mathbf{U}\right) \approx \frac{d\mathbf{U}_g}{dt},$$

$$\frac{d\mathbf{U}_g}{dt} = \frac{\partial \mathbf{U}_g}{\partial t} + \mathbf{U} \cdot \nabla_\theta \mathbf{U}_g, \qquad (2)$$

[4] Numerical model simulations discussed in the paper by Uccellini *et al.* (1983) show that the divergence maximum developed in the Middle Atlantic states between 03Z/18 and 09Z/18, while the divergence field in Illinois moved slowly eastward.

has served as a mathematical basis for the observations of transverse circulations near jet streaks (e.g., Uccellini and Johnson, 1979) and is used to approximate the ageostrophic, horizontal branches of the transverse circulation, with

$$\mathbf{U}_{ag} \approx f^{-1}\left[\mathbf{k} \times \frac{\partial \mathbf{U}_g}{\partial t} + \mathbf{k} \times \mathbf{U} \cdot \nabla_\theta \mathbf{U}_g\right]. \quad (3)$$

The first term in (3) is the isallobaric term, which usually dominates in the lower-tropospheric return branch (Uccellini and Johnson, 1979). The second term is the inertial-advective term, which is assumed to dominate in the upper troposphere (Bjerknes, 1951).

As noted by Hoskins (1975), the geostrophic momentum approximation represents an improvement over the quasi-geostrophic approximation for studying ageostrophic flow near jets, since the total wind, rather than the geostrophic wind, is used to advect geostrophic momentum in the inertial-advective term. However, Shapiro and Kennedy (1981) have shown that the geostrophic momentum approximation can become inaccurate for jet streaks situated in the base of a trough with significant cyclonic curvature.

Several points were chosen along the axis of the STJ in order to compare total parcel accelerations with those approximated by (2). The parcel accelerations used in this evaluation are derived from the trajectory illustrated in Fig. 12 and listed in Table 1 for points P, R, and S in Fig. 10B and Fig. 12. The sign of the local derivative of $\mathbf{U}$ and $\mathbf{U}_g$ in (2) is evaluated from the linear change measured over a 12 h period. The sign of the inertial-advective term is determined from the 332 K total and geostrophic wind analyses closest to the time interval used to evaluate the parcel accelerations.

The results of the evaluation are listed in Table 2. At point P, the parcel acceleration into the STJ is approximated fairly well by the geostrophic momentum approximation with both the isallobaric and inertial-advective terms contributing to the acceleration. In contrast, the approximation is unsatisfactory at point R where the acceleration approximated by the geostrophic wind is of opposite sign to the acceleration based on the total wind. Therefore, the ageostrophic components derived from (3) would be opposite in sign to the observed ageostrophic component. At point S, the parcel acceleration is again approximated satisfactorily by the geostrophic momentum approximation, although the contributions by the individual terms do not entirely agree in that the positive local tendency for the total wind is matched by a positive inertial-advective term based on the geostrophic wind.

The failure of the geostrophic momentum approximation at point R occurred at the beginning of the second acceleration experienced by parcels passing through the STJ (Fig. 11) and where 20 m s^{-1} ageostrophic winds directed toward the cyclonic side of the STJ were diagnosed (Fig. 10C). *The total wind speed for the parcel increased by 3.2 m s^{-1} over 3 h as the geostrophic wind speed decreased by 8.2 m s^{-1}.* This breakdown in the geostrophic momentum approximation at R is linked directly to the misrepresentation of the inertial-advective term in (2) (see Table 2). In terms of the geostrophic momentum approximation, the parcel located at R is in the exit region or downwind of the geostrophic wind maximum (Fig. 10B). Thus, U_g decreases in the along-stream direction and the inertial-advective term using the geostrophic wind is negative. However, in terms of the total wind, the parcel is still in the entrance region (Fig. 10A) where the inertial-advective term is positive. The misrepresentation of the inertial-advective term in (2) by the geostrophic momentum approximation in the region upwind of the ridge axis is related to the 700 km displacement between the actual wind maximum and the geostrophic wind maximum (Fig. 10).

The contribution of the inertial-advective term to the breakdown of the geostrophic momentum approximation near the ridge can be represented by an evaluation of the Rossby Number (Ro), where

$$\mathrm{Ro} = \frac{|d\mathbf{U}/dt|}{f|\mathbf{U}|}$$

is approximated by

$$\mathrm{Ro} \approx \frac{|\mathbf{U} \cdot \nabla_\theta \mathbf{U}|}{f|\mathbf{U}|}, \quad (4)$$

which neglects the local tendency of $\mathbf{U}$. Fig. 14 illus-

TABLE 2. Evaluation of wind speed change following a parcel (ΔU), local wind change ($\partial \mathbf{U}/\partial t$) and inertial-advective term ($\mathbf{U} \cdot \nabla_\theta \mathbf{U}$) for points P, R and S shown in Fig. 10B, and comparison with the respective terms based upon the geostrophic momentum approximation in (2). Data for ΔU and ΔU_g derived from parcel trajectory listed in Table 1, (t_0, t_1) represents time interval (h) over which changes in total (ΔU) and geostrophic (ΔU_g) wind speeds (m s^{-1}) are measured. Contribution of local tendencies and inertial-advective terms are derived for sign only using 332 K analysis (Fig. 10) for times shown.

Point	(t_0, t_1)	ΔU	ΔU_g	$\partial U/\partial t$	$\partial U_g/\partial t$	$\mathbf{U} \cdot \nabla_\theta \mathbf{U}$	$\mathbf{U} \cdot \nabla_\theta \mathbf{U}_g$	
P	3 h, 6 h	+8.7	+7.3	>0	>0	>0	>0	(00Z/18)
R	8.5 h, 10.5 h	+3.2	−8.2	>0	≈0	>0	<0	(12Z/18)
S	10.5 h, 12.0 h	+3.5	+6.9	>0	≈0	≈0	>0	(12Z/18)

trates that Ro approached unity[5] at 12Z/18, when both the cross-stream ageostrophic winds (Fig. 10C) and increasing upper-level divergence (Fig. 13) were diagnosed upwind of the ridge axis. This result is yet another indication of unbalanced flow and agrees with Blumen's (1972) discussion of the failure of the quasi-geostrophic and geostrophic momentum approximations near the axis of jet streaks where Ro is large. The analysis also expands upon Shapiro and Kennedy's (1981) discussion on the limitations of the geostrophic momentum approximation for sharply curved, cyclonic flow situations in that the approximation can also fail for cases of relatively straight flow and moderate anticyclonic curvature in the geopotential field.

4. A Description of the mass adjustments, transverse circulation and the development of the first area of heavy snow near the STJ

In Section 3, the flow in the STJ was found to be increasingly supergeostrophic and possibly unbalanced as it propagated toward the East Coast between 12Z/17 and 12Z/18. In this section, the effects of the intensification of the STJ on the mass adjustments and a transverse circulation near the jet core are discussed and then related to the development of the first area of heavy snow in the southeastern United States at 12Z/18.

a. Mass adjustments, vertical velocity, and transverse circulation associated with the STJ

The impact of the ageostrophic flow on the mass divergence is examined using the hydrostatic version of the continuity equation in isentropic coordinates,

$$\frac{\partial}{\partial t}\left(\frac{\partial p}{\partial \theta}\right) = -\left[\nabla_\theta \cdot \left(\frac{\partial p}{\partial \theta}\mathbf{U}\right) + \frac{\partial}{\partial \theta}\left(\frac{\partial p}{\partial \theta}\frac{d\theta}{dt}\right)\right]. \quad (5)$$

The two terms on the right in (5) represent the adiabatic and diabatic contributions to the mass tendencies, respectively. The total adiabatic mass flux divergence can be partitioned further into geostrophic (A) and ageostrophic (B) components by:

$$\nabla_\theta \cdot \left(\frac{\partial p}{\partial \theta}\mathbf{U}\right) = \nabla_\theta \cdot \left(\frac{\partial p}{\partial \theta}\mathbf{U}_g\right) + \nabla_\theta \cdot \left(\frac{\partial p}{\partial \theta}\mathbf{U}_{ag}\right)$$

$$= \mathbf{U}_g \cdot \nabla_\theta \frac{\partial p}{\partial \theta} + \nabla_\theta \cdot \left(\frac{\partial p}{\partial \theta}\mathbf{U}_{ag}\right). \quad (6)$$

(A) (B)

For term (A), it is assumed that the divergence of $\mathbf{U}_g$ is negligible.

[5] It was not possible to combine an evaluation of $\partial \mathbf{U}/\partial t$ and $\mathbf{U} \cdot \nabla_\theta \mathbf{U}$ in the computation of Ro given the 12 h time increment in the radiosonde data set. Since $\partial \mathbf{U}/\partial t$ and $\mathbf{U} \cdot \nabla_\theta \mathbf{U}$ have the same sign along the axis of the STJ for this case, the maximum values of Ro immediately upwind of the jet core in Fig. 14 are probably a slight underestimate.

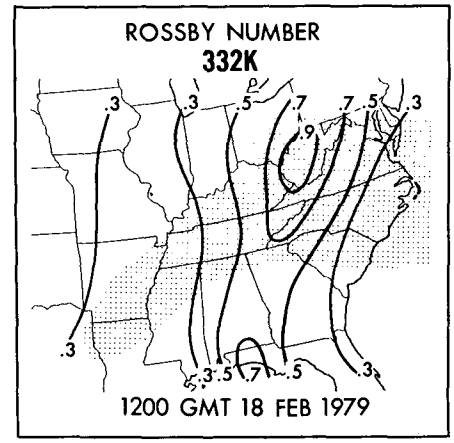

FIG. 14. Rossby Number for 332 K surface at 1200 GMT 18 February 1979. Shaded area represents region in which winds are greater than 70 m s^{-1}. See text for method of computation.

Area-averaged profiles of the total, geostrophic and ageostrophic mass divergence were computed using (6) at 00Z/18 and 12Z/18 for the regions shown in Fig. 15. Areas A and C are located near the axis of the STJ, and were selected to represent the region upstream of the ageostrophic wind maximum. Areas B and D are positioned to the right of the jet axis. At 00Z/18 and 12Z/18, upper-level mass convergence is diagnosed to the right of the STJ above 600 mb (profiles B and D). Along the axis of the STJ, mass divergence is observed between 200 and 400 mb at both times (profiles A and C), although the divergence is relatively weak at 00Z/18. Below 500 mb, a reversal is evident in both sets of profiles, although the lower-tropospheric mass convergence below the jet axis is not well defined at 00Z/18 (profile A).

By 12Z/18, a significant increase in the magnitude of the upper-level mass divergence occurred along the axis of the STJ between 225 and 425 mb (profile C). The increase in the mass divergence was dominated by the ageostrophic component and related to the amplification of the *along- and cross-stream* components of the ageostrophic flow as the STJ propagated toward the East Coast and amplified near the ridge crest (Fig. 10C). To the right of the STJ, the upper-level mass convergence increased slightly between 00Z/18 and 12Z/18 with nearly equal ageostrophic and geostrophic components (profile D), indicating that the geostrophic advection of mass into this area was also an important factor in the mass convergence diagnosed along the Southeast Coast.

The low-level mass convergence beneath the STJ also increased in between 00Z/18 and 12Z/18 and was dominated by the ageostrophic component. The dominance of the ageostrophic mass divergence and convergence in the lower troposphere at 12Z/18 at profiles C and D, respectively, appears to be related to the development of the highly ageostrophic LLJ along the

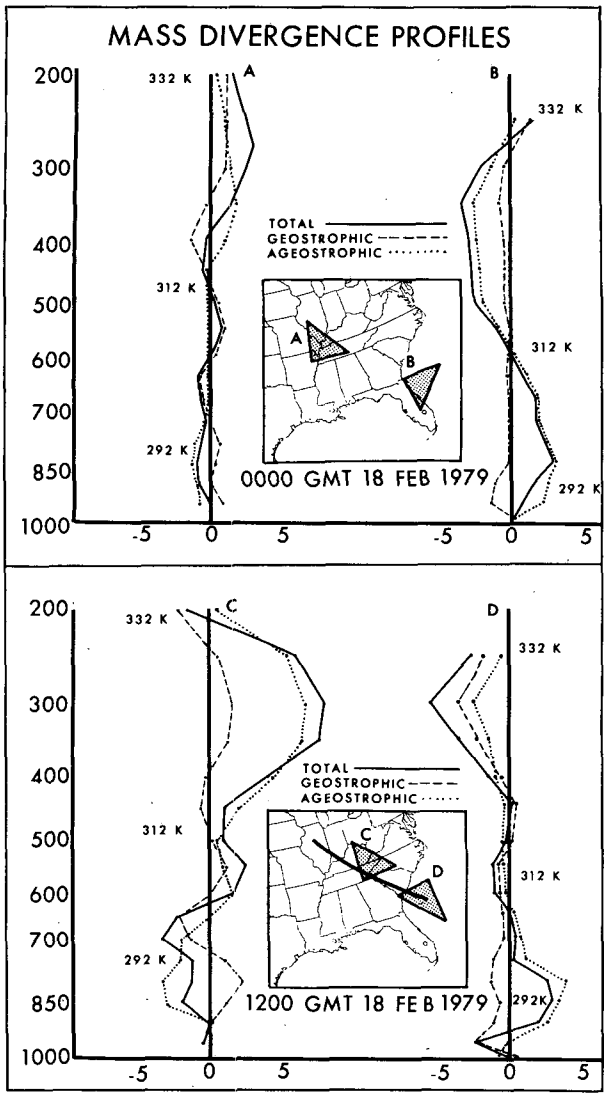

FIG. 15. Profiles of total (solid), geostrophic (dashed) and ageostrophic (dotted) mass divergence at 0000 GMT 18 February 1979 (top) and 1200 GMT 18 February 1979 (bottom). ($-5 = -5 \times 10^{-5}$ mb s^{-1} K^{-1}). The profiles are computed along and to the anticyclonic side of the STJ over the shaded regions depicted on the map inserts. Line running through map insert represents axis of cross section shown in Fig. 16.

Southeast Coast (Fig. 4C1). An additional, shallow layer of mass convergence below 900 mb along the East Coast (profile D) appears to be a reflection of the coastal frontogenesis occurring at 12Z/18.

The two-layer structure of the mass divergence profiles C and D in Fig. 15 suggests rising motion along the axis of the STJ and sinking motion to the right of the jet. To verify this pattern, vertical velocities ($\omega = dp/dt$) were computed in the following manner. First, the winds on isentropic surfaces were interpolated to pressure surfaces at 50 mb intervals. The ω fields were then derived by vertically integrating the continuity equation in pressure coordinates with the two constraints described by O'Brien (1970): 1) the variance of the error in divergence is assumed to increase linearly with decreasing pressure and 2) ω at 125 mb is zero. The ω fields were then interpolated from the grid points to the cross-section plane nearly normal to the axis of the STJ (Fig. 15). The adjusted divergence and computed ω at 12Z/18 are shown in Fig. 16A.

To the right of the STJ, where mass convergence (mass divergence) was diagnosed in the upper (lower) troposphere, there is sinking motion approaching 6 μb s^{-1}. Along the axis of the STJ, where mass divergence (mass convergence) was diagnosed in the upper (lower) troposphere, rising motion exceeded 8 μb s^{-1}. The vertical motion pattern (Fig. 16A) with rising (sinking) motion in the relatively colder (warmer) air indicates that a thermodynamically indirect transverse circulation existed near the STJ. To complete the description of the transverse indirect circulation, a cross section of the component of the ageostrophic wind tangent to the cross-sectioned plane is shown in Fig. 16B. In the upper troposphere, a 10–15 m s^{-1} ageostrophic component was directed to the right of the STJ, while in the lower troposphere, a 15–20 m s^{-1} ageostrophic component was directed to the left. The cross sections of ω and the ageostrophic wind normal to the STJ clearly depict the horizontal and vertical branches of the indirect circulation on the anticyclonic side of the STJ.

The mass divergence profiles (Fig. 15) and the existence of an indirect circulation agree with Rossby's (1949), Matsumoto's (1961), and Chen's (1982) descriptions of the mass adjustments needed to increase the slope of isentropic surfaces below the axis of a supergeostrophic current to generate the baroclinic support, while simultaneously diminishing the total wind speed in the jet to restore balance to the supergeostrophic flow. In this case, the mass adjustments acted to enhance the ψ_m gradients beneath the axis of the STJ, *especially during the 12 h period after 12Z/18* as the geostrophic wind near the jet core increased markedly to 80 m s^{-1} by 00Z/19 (Fig. 6B).

Nevertheless, the indirect circulation to the right of the STJ displays several characteristics which deviate from the pattern described by Rossby (1949), Reiter (1969), and Uccellini and Johnson, (1979). The indirect circulation was shifted noticeably to the anticyclonic side of the STJ *with the rising branch maximized beneath the axis of the STJ, and even on the anticyclonic side of the jet below 500 mb, rather than on the cyclonic side.* The shift of the indirect circulation toward the right side of the STJ could be related to smaller values of absolute vorticity associated with the anticyclonic shear and curvature, as discussed by Bjerknes (1951). The indirect circulations were also diagnosed near the jet core at 12Z/18, rather than existing entirely within the exit region of the jet streak. Furthermore, the upper-level ageostrophic component *directed to the left of the STJ near the jet axis* (Fig. 16B) deviates from previous,

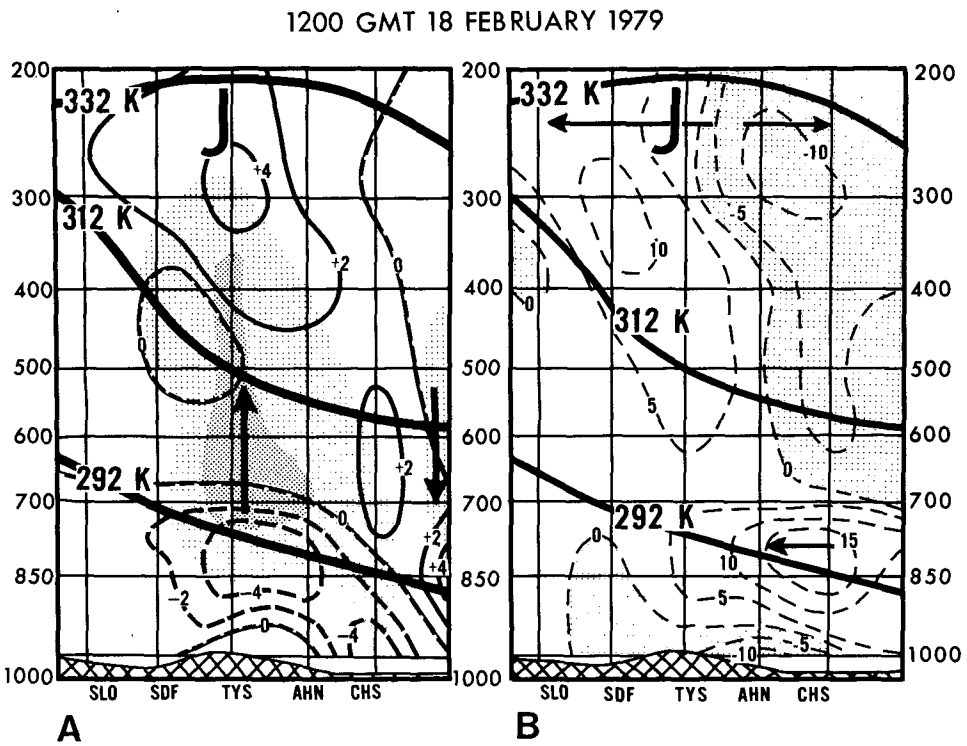

FIG. 16. (A) Cross section (see inset map in Fig. 15) of divergence adjusted according to O'Brien scheme described in text (dashed line is convergence, solid line is divergence; 10^{-5} s^{-1}), and vertical motion (with values greater or less than ± 4.0 μb s^{-1} shaded lightly and ± 8.0 μb s^{-1} shaded more heavily) from northern Illinois to the Southeast Coast at 1200 GMT 18 February 1979. Arrows indicate rising and sinking motion. (B) Cross section of the horizontal component of the ageostrophic wind in the plane of the cross section at 1200 GMT 18 February 1979 (dashed, m s^{-1}; positive values are directed to the left; negative values (shaded) are directed to the right). J represents location of STJ. Solid lines represent 292, 312 and 332 K isentropes.

idealized descriptions of transverse circulations in regions where the flow is supergeostrophic and *was a dominant factor for the upper-level mass divergence patterns near the axis of the STJ.* Finally, the along-stream ageostrophic components also contributed to the mass divergence and vertical motions beneath the axis of the STJ. Thus, while the transverse circulation is depicted on a two-dimensional vertical plane (Fig. 16), the existence of the indirect circulation and associated mass adjustments was the consequence of three-dimensional variations in the ageostrophic winds and upper-level divergence that cannot be described in terms of simple, two-dimensional, straight-line jet streak dynamics.

The development of the LLJ along the Southeast Coast (Fig. 4C1) appears to occur within the lower branch of the indirect circulation where the magnitude of the ageostrophic winds was greater than 15 m s^{-1} (Fig. 16B). The formation of the LLJ within the lower branch of the indirect circulation and the two-layer mass divergence profiles along and to the right of the STJ (Figs. 15C and 15D) suggests that a coupling between the STJ and LLJ (Uccellini and Johnson, 1979) might be linked to the mass adjustments associated with the STJ. However, diabatic and boundary layer processes were also contributing to the development of the LLJ for this case (Uccellini *et al.*, 1983).

b. Influence of the STJ and LLJ on the development of heavy snow

It appears that the STJ had considerable influence on the development of the first area of heavy snow in the southeastern United States between 00Z/18 and 12Z/18 (Fig. 1). The increase in the upper-level mass divergence and the associated increase of upward vertical motion to greater than 8 μb s^{-1} near the axis of the STJ (Fig. 16A) coincided with the cloud shield over the southeastern United States (Fig. 8) and the heavy snowfall at 12Z/18 (Fig. 1). These results suggest that significant upper-level forcing for the development of heavy snow existed near the ridge at 12Z/18 in the Southeast even though the trough axis was still located in the central part of the United States. This finding is consistent with those which have linked the interaction of jet streaks and upper-level ridges to an increase in the upper-level divergence for cases of organized severe convective storms through an evaluation of the divergence equation (House, 1961; Paine *et al.*, 1975; Kaplan and Paine, 1977).

The development of the LLJ within the return branch of the indirect circulation also appears to have had considerable influence on the heavy snowfall near the East Coast through 1) the low-level convergence and vertical motion downwind of the LLJ (Fig. 16A), and 2) the rapid transport of moisture into the area of heavy snow for three consecutive times (Table 3). The moisture transport ($\rho\bar{q}\bar{V}$) in Table 3 was computed for selected soundings along the axis of the LLJ, where q is the mixing ratio, ρ is density, V is the wind component along the axis of the LLJ, and the overbar indicates an average over a 50 mb layer in the individual soundings. Between 00Z/18 and 12Z/18, the moisture flux along the Southeast Coast and directed toward the area of heavy snow doubled from 60 to 125×10^{-3} kg m^{-2} s^{-1} as the low-level winds increased to 25 m s^{-1}. This value compares favorably with moisture transports associated with a LLJ in a spring-time, convective environment (Uccellini and Johnson, 1979). As the LLJ propagated slowly northward along the coast between 12Z/18 and 12Z/19, it continued to transport moisture into the area of heavy snow at rates exceeding 100×10^{-3} kg m^{-2} s^{-1} as the cyclone began to develop between 00Z/19 and 12Z/19. The LLJ also may have contributed to the pressure falls and subsequent development of the inverted trough along the East Coast after 12Z/18 (Figs. 1C and 1D) by increasing the warm air advection along the coast. It therefore appears that the STJ and LLJ combined to contribute to the heavy snowfall on 18 February and to a more favorable environment for the subsequent cyclogenesis along the coast through increased divergence aloft and enhanced warm air advection and moisture transports in the lower troposphere.

5. Summary

The analyses of the Presidents' Day cyclone presented in this paper and those of Bosart (1981) show that a combination of complex dynamical and physical processes was responsible for establishing conditions favorable for the development of the intense storm that produced snowfall rates up to 12 cm h^{-1}. A synoptic-scale upper-tropospheric wave and three distinct jet streaks appear to have been important ingredients in the development of this storm. Boundary-layer processes associated with cold air damming, sensible heat transport over the ocean, and latent heat release also influenced the rapid development of the cyclone within a limited area.

Specific findings from the analyses in this paper include:

1) Two systems were responsible for the heavy snowfall in the eastern United States. A region of heavy snow in the southeastern United States on 12Z/18 February was associated with an intensifying subtropical jet streak, a developing low-level jet, and, as Bosart has shown, the effects of cold air damming to the lee of the Appalachians and coastal frontogenesis. The second area of heavy snow that developed as cyclogenesis commenced along the East Coast on 19 February was related to an upper-tropospheric trough and a polar jet streak propagating eastward from the Ohio Valley, combined with the pre-existing coastal front and inverted trough.

2) Prior to the development of the intense cyclone off the East Coast, the maximum wind speeds associated with the STJ increased by 15 to 20 m s^{-1} between 12Z/17 and 12Z/18 February 1979 as the jet propagated toward the eastern United States. During this period, the intensifying STJ was found to be increasingly supergeostrophic near the crest of a slowly moving ridge, especially at 12Z/18. There is also evidence to suggest that the STJ was becoming increasingly unbalanced during the same period. The divergence along the axis of the STJ increased as the wavelength of the trough–ridge system decreased, the cross-contour ageostrophic flow increased, and the Rossby Number approached unity. These signals agree with a) Bjerknes' (1954) criteria for unbalanced, nongradient flow at a ridge crest, b) House's (1961), Paine *et al.* (1975), and Kaplan and Paine's (1977) description of unbalanced flow in which divergence increases with time, c) Newton's (1981) discussion of the nongradient aspects of a STJ associated with a short wavelength trough–ridge system, and Van Tuyl and Young's (1982) designation of the temporally increasing divergence along the axis of the jet as an indication for unbalanced flow. The large divergence tendency experienced by parcels passing through the jet core indicates that the assumption needed to derive the balance equation [$d(\nabla \cdot \mathbf{U})/dt$ is negligible] would not be satisfied for the STJ at 12Z/18.

TABLE 3. Moisture transport along axis of low-level jet averaged over 900 to 850 mb layer for soundings indicated. Mean wind direction DD (deg), wind speed FF (m s^{-1}) and mixing ratio q (g kg^{-1}) are averaged over the 900–850 mb layer.

Time	Location of LLJ	Sounding	DD	FF	q	Moisture transport (kg m^{-2} s^{-1})
00Z/18	none	Waycross, Georgia*	170	08	7.6	60.0×10^{-3}
12Z/18	South Carolina coast	Charleston, South Carolina	130	25	5.0	125.0×10^{-3}
00Z/19	North Carolina coast	Hatteras, North Carolina	130	21	5.0	105.0×10^{-3}
12Z/19	Virginia coast	Wallops Island, Virginia	140	24	4.5	112.0×10^{-3}

* No significant level data available.

3) The combination of the increasing confluence in the entrance region of the STJ and the decreasing wavelength of the trough–ridge pattern along the jet axis contributed to the intensifying and apparently unbalanced flow in the STJ near a ridge crest. Supergeostrophic parcels approached the ridge axis with a wind speed that was too large in a time period that was too short to follow the ψ_m contours around the ridge crest. Rather, parcels moving along the axis of the STJ propagated through the ridge, were directed toward lower ψ_m values, continued to accelerate, and become increasingly supergeostrophic.

4) Analysis of the ageostrophic flow and parcel accelerations based on the use of geostrophic momentum approximations failed to adequately describe the ageostrophic structure of the amplifying STJ at 12Z/18 February when the jet had attained its maximum wind speed and was becoming increasingly unbalanced. The ageostrophic component directed toward lower ψ_m values immediately upwind of the ridge axis was *opposite* to the pattern defined by the geostrophic momentum approximation. The inaccuracy of this approximation is related to the displacement between the location of the wind maximum at the ridge crest and the geostrophic wind maximum 700 km upstream of the ridge axis.

5) A transverse indirect circulation was diagnosed on the anticyclonic side of the STJ with maximum upward vertical motion between 400 and 700 mb directly beneath the jet core and generally below 500 mb on the anticyclonic side of the STJ, rather than on the cyclonic side of the jet as would be expected for straight, finite length and nearly balanced jet streaks. The existence of the indirect circulation was related to the three-dimensional structure of the ageostrophic winds near the axis of the STJ and could not be described in terms of two-dimensional straight-line jet streak dynamics based on the geostrophic momentum approximation.

6) The STJ and LLJ had significant influence on the pre-cyclogenetic environment. The temporally increasing upper-level mass divergence and upward vertical motion near the axis of the STJ coincided with the development of the first area of heavy snow. The low-level convergence, moisture flux, and warm air advection associated with the development of the LLJ along the Southeast Coast also had a considerable effect. The increased moisture transport and low-level convergence aided the development of heavy snowfall. The warm air advection contributed to the low-level pressure falls and subsequent development of the inverted trough immediately along the coast. Thus, the upper-level divergence associated with the STJ and the warm air advection associated with the LLJ appeared to prime the East Coast for the rapid cyclogenesis commencing on 19 February.

Important questions remain for future research. The issue of initializing regional-to-mesoscale models in situations containing unbalanced flows, which do not satisfy the balance constraints often applied to initial wind fields, has already been raised (Van Tuyl and Young, 1982). Other questions concern 1) the role of the tropopause fold on the development of the cyclone, 2) the contributions of diabatic processes related to latent and sensible heating along the East Coast on the amplifying jet streak circulations and on the cyclogenesis, 3) the reasons why the ridge remained nearly stationary over the eastern United States as the trough propagated through the Midwest and 4) the possible role that the STJ and LLJ might have played in the development of the coastal front. Finally, the results from this case study may be applicable to other examples of heavy precipitation near upper-tropospheric ridges, such as the recent snowstorm over southeastern Wales and neighboring parts of England on 8 and 9 January 1982 (Browning, 1983) and mesoscale convective complexes (Maddox, 1983). Although a well-defined jet streak is not always necessary for the development of a mesoscale convective complex, many cases are marked by a weak trough and an area of stronger winds immediately upwind of the ridge axis (Maddox and Deitrich, 1982). The similarity between the diagnoses of the divergence, mass divergence and vertical motions associated with the STJ in this case and evaluations of the divergence equation for other cases of severe storms suggests that the acceleration of parcels approaching a ridge axis and the associated increase in the upper-level divergence could be sufficient to initiate the convection in areas where the potential static stability is low. An examination of these issues through analytical, numerical and observational studies can provide additional insight into the nonlinear, scale interactive processes leading to severe winter cyclones and spring convective storms producing heavy precipitation.

Acknowledgments. We gratefully acknowledge the following people who have aided in our analysis of the Presidents' Day Cyclone: Mr. Thomas Whittaker of the Space Science and Engineering Center (SSEC) at the University of Wisconsin for his assistance with processing the RAOB data, and Miss Kelly Wilson for typing the countless drafts of the manuscript. We thank Dr. J. Paegle, whose FGGE analyses for this period encouraged us to continue our efforts in this case study. We also thank Drs. Daniel Keyser and Chester W. Newton whose thorough reviews were very helpful in shaping the final version of this paper. Discussions with Dr. Robert Atlas, Dr. Michael Kaplan, and Mr. Michael Pecnick were also helpful during the course of the case study. This work was partially supported by the National Science Foundation through Grants 7722976, ATM 80-13636 and by the Naval Postgraduate School through support of the Office of Naval Research.

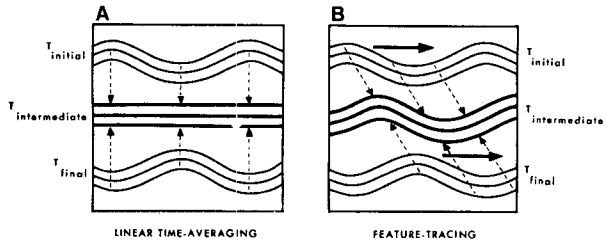

FIG. 17. Schematic illustrating impact of interpolation of wave features at an intermediate time (A) using linear ψ_m tendencies only, (B) using a wave-tracing technique.

APPENDIX

Trajectory Computation

The procedure used to produce the trajectories differs in one respect from that already in the literature (Petersen and Uccellini, 1979). As was previously noted by Petersen and Uccellini (1979), there are limitations to their explicit approach and Danielsen's (1961) implicit approach when computing trajectories using the operational data base. The greatest problem is the 12 h time interval between radiosonde soundings, which affects the computation of the local ψ_m tendency needed for either scheme. In cases of fast-moving waves, the assumption that the Montgomery stream function ψ_m at each grid point varies linearly in time produces a time evolution in which ψ_m gradients may be underestimated or misrepresented between observation times, as illustrated in Fig. 17. With the linear assumption imposed on the ψ_m tendencies, waves are assumed to dissipate at their initial locations and redevelop at the final locations without propagating yielding a ψ_m field at an intermediate time which significantly misrepresents the mass distribution (Fig. 17A). To alleviate this deficiency, initial and final positions of geostrophic vorticity extrema are used to identify significant wave features in the flow and then to measure the progression of the waves in order to obtain a spatially varying field of wave translation rates. At each time step, the features in the initial ψ_m field are moved linearly ahead in time and the final features are moved backwards using the translation rate at the parcel locations. The two translated ψ_m fields are then averaged to obtain ψ_m gradients at each parcel location. In this manner, the amplitudes of the waves are preserved at intermediate times (Fig. 17B). Other deficiencies in this scheme include the lack of terms involving the earth's curvature, viscous forces and diabatic processes, all of which could affect the actual trajectory.

REFERENCES

Beebe, R. G., and F. C. Bates, 1955: A mechanism for assisting in the release of convective instability. *Mon. Wea. Rev.*, **83,** 1–10.

Bjerknes, J., 1951: Extratropical cyclones. *Compendium of Meteorology,* T. F. Malone, Ed., Amer. Meteor. Soc., 577–598.

——, 1954: The diffluent upper trough. *Arch. Meteor. Geophys. Bioklim.,* Series A, **7,** 41–46.

Blumen, W., 1972: Geostrophic adjustment. *Rev. Geophys. Space Phys.,* **10,** 485–528.

Bosart, L. F., 1981: The Presidents' Day snowstorm of 18–19 February 1979: A subsynoptic-scale event. *Mon. Wea. Rev.,* **109,** 1542–1566.

Browning, K. A., 1983: Air motion and precipitation growth in a major snowstorm. *Quart. J. Roy. Meteor. Soc.,* **109,** 225–242.

Carlson, T. N., 1980: Airflow through midlatitude cyclones and the comma cloud pattern. *Mon. Wea. Rev.,* **108,** 1498–1509.

Chen, Q., 1982: The instability of the gravity-inertia wave and its relation to low-level jet and heavy rainfall. *J. Meteor. Soc. Japan,* **60,** 1041–1057.

Danielsen, E. F., 1961: Trajectories: Isobaric, isentropic and actual. *J. Meteor.,* **18,** 479–486.

Eliassen, A., 1948: The quasi-static equations of motion with pressure as an independent variable. *Geofys. Publ.,* **17**(3), 1–44.

Endlich, R. M., 1961: Computation and uses of gradient winds. *Mon. Wea. Rev.,* **89,** 187–191.

——, and G. S. McLean, 1960: Geostrophic and gradient departures in jet streams. *J. Meteor.,* **17,** 135–147.

Foster, J. L., and R. J. Leffler, 1979: The extreme weather of February 1979 in the Baltimore–Washington area. *Nat. Wea. Digest,* **4,** 16–21.

Haltiner, G. J., and F. L. Martin, 1957: *Dynamic and Physical Meteorology.* McGraw-Hill, Chap. 12.

Hoskins, B. J., 1975: The geostrophic momentum approximation and the semi-geostrophic equations. *J. Atmos. Sci.,* **32,** 233–242.

House, D. C., 1961: The divergence equation as related to severe thunderstorm forecasting. *Bull. Amer. Meteor. Soc.,* **42,** 803–816.

Hovanec, R. D., and L. H. Horn, 1975: Static stability and the 300 mb isotach field in the Colorado cyclogenetic area. *Mon. Wea. Rev.,* **103,** 628–638.

Kaplan, M. A., and D. A. Paine, 1977: The observed divergence of the horizontal velocity field and pressure gradient force at the mesoscale. Its implications for the parameterization of three-dimensional momentum transport in synoptic-scale numerical models. *Beitr. Phys. Atmos.,* **50,** 321–330.

Krishnamurti, T. N., 1961: The subtropical jet stream of winter. *J. Meteor.,* **18,** 172–191.

Maddox, R. A., 1983: Large-scale meteorological conditions associated with midlatitude mesoscale convective complexes. *Mon. Wea. Rev.,* **111,** 1475–1493.

——, and W. Deitrich, 1982: Meteorological settings associated with simultaneous occurrences of severe thunderstorms and flash floods. *Nat. Wea. Digest,* 7(3), 36–43.

Matsumoto, S., 1961: A note on geostrophic adjustment and gravity wave in the atmosphere. *J. Meteor. Soc. Japan,* **39,** 18–28.

Murray, R., and S. M. Daniels, 1953: Transverse flow at entrance and exit to jet streams. *Quart. J. Roy. Meteor. Soc.,* **79,** 236–241.

Namias, J., and P. F. Clapp, 1949: Confluence theory of the high tropospheric jet stream. *J. Meteor.,* **6,** 330–336.

Newton, C. W., 1956: Mechanism of circulation change during a lee cyclogenesis. *J. Meteor.,* **13,** 528–539.

——, 1959: Axial velocity streaks in the jet stream: Ageostrophic "inertial" oscillations. *J. Meteor.,* **16,** 638–645.

——, 1981: Lagrangian partial-inertial oscillations, and subtropical and low-level monsoon jet streaks. *Mon. Wea. Rev.,* **109,** 2474–2486.

——, and A. V. Persson, 1962: Structural characteristics of the subtropical jet stream and certain lower-stratospheric wind systems. *Tellus,* **14,** 221–241.

O'Brien, J. J., 1970: Alternative solutions to the classical vertical velocity problem. *J. Appl. Meteor.,* **9,** 197–203.

Oliver, V. J., and M. B. Oliver, 1951: Meteorological analysis in the middle latitudes. *Compendium of Meteorology,* T. F. Malone, Ed., Amer. Meteor. Soc., 715–727.

Paine, D. A., J. W. Zack, J. T. Moore and R. J. Posner, 1975: A theory for the conservation of three-dimensional vorticity which describes the cascade of energy–momentum leading to tornadic vortices. Ninth Conf. Severe Local Storms, Norman, Amer. Meteor. Soc., 131–138.

Palmén, E., and C. W. Newton, 1969: *Atmospheric Circulation Systems.* Academic Press, 603 pp.

Petersen, R. A., 1979: A cross sectional approach to three-dimensional analysis. *Fourth Conf. Numerical Weather Prediction,* Silver Spring, Amer. Meteor. Soc., 35–42.

——, and L. W. Uccellini, 1979: The computation of isentropic atmospheric trajectories using a "discrete model" approach. *Mon. Wea. Rev.,* **107,** 566–574.

Petterssen, S., 1956: *Weather Analysis and Forecasting, Vol. 1.* McGraw-Hill, Chap. 4.

Platzman, G. W., 1947: Some remarks on the measurement of curvature and vorticity. *J. Meteor.,* **4,** 58–62.

Reed, R. J., and E. F. Danielsen, 1959: Fronts in the vicinity of the tropopause. *Arch. Meteor. Geophys. Bioklim.,* **11,** 1–17.

Reiter, E. R., 1969: Tropopause circulation and jet streams. *World Survey of Climatology,* Vol. 4, *Climate of the Free Atmosphere,* D. F. Rex, Ed., Elsevier, 85–193.

Richwien, B. A., 1980: The damming effect of the southern Appalachians. *Nat. Wea. Digest,* **5,** 2–12.

Riehl, H., and Collaborators, 1952: *Forecasting in the Middle Latitudes. Meteor. Monogr.,* No. 5, Amer. Meteor. Soc., 80 pp.

Rossby, C.-G., 1949: On the nature of the general circulation of the lower atmosphere. *The Atmosphere of the Earth and Planets,* G. P. Kuiper, Ed., The University of Chicago Press, 16–48.

Scofield, R. A., V. J. Oliver and L. E. Spayd, 1982: Preliminary efforts in developing a technique that uses satellite data for analyzing precipitation from extratropical cyclones. *Ninth Conf. Weather Forecasting and Analysis,* Seattle, Amer. Meteor. Soc., 235–244.

Shapiro, M. A., 1976: The role of turbulence heat flux in the generation of potential vorticity in the vicinity of upper-level jet stream systems. *Mon. Wea. Rev.,* **104,** 892–906.

——, and P. J. Kennedy, 1981: Research aircraft measurements of jet stream geostrophic and ageostrophic winds. *J. Atmos. Sci.,* **38,** 2642–2652.

Staley, D. O., 1960: Evaluation of potential-vorticity changes near the tropopause and related vertical motions, vertical advection of vorticity, and transfer of radioactive debris from stratosphere to troposphere. *J. Meteor.,* **17,** 591–620.

Uccellini, L. W., 1976: Operational diagnostic applications of isentropic analysis. *Nat. Wea. Digest,* **1,** 4–12.

——, and D. R. Johnson, 1979: The coupling of upper- and lower-tropospheric jet streaks and implications for the development of severe convective storms. *Mon. Wea. Rev.,* **107,** 682–703.

——, P. J. Kocin and C. H. Wash, 1981: The Presidents' Day Cyclone 17–19 February 1979: An analysis of jet streak interactions prior to cyclogenesis. NASA Tech. Memo 82077, Goddard Space Flight Center, Greenbelt, MD, 59 pp. [NTIS 81N20658]

——, R. A. Petersen, P. J. Kocin, M. J. Kaplan, J. W. Zack and V. C. Wong, 1983: Mesoscale numerical simulations of the Presidents' Day cyclone: Impact of sensible and latent heating on the pre-cyclogenetic environment. *Sixth Conf. Numerical Weather Prediction,* Amer. Meteor. Soc., 45–52.

Van Tuyl, A. H., and J. A. Young, 1982: Numerical simulation of nonlinear jet streak adjustment. *Mon. Wea. Rev.,* **110,** 2038–2054.